PLOS PATHOGENS

RESEARCH ARTICLE

Inhibition of anti-viral stress granule formation by coronavirus endoribonuclease nsp15 ensures efficient virus replication

Bo Gao[1☯], Xiaoqian Gong[1,2☯], Shouguo Fang[3], Wenlian Weng[1], Huan Wang[1], Hongyan Chu[1], Yingjie Sun[1], Chunchun Meng[1], Lei Tan[1], Cuiping Song[1], Xusheng Qiu[1], Weiwei Liu[1], Maria Forlenza[2], Chan Ding[1,4], Ying Liao[1]*

1 Department of Avian Diseases, Shanghai Veterinary Research Institute, Chinese Academy of Agricultural Sciences, Shanghai, P. R. China, **2** Cell Biology and Immunology Group, Department of Animal Sciences, Wageningen University, Wageningen, The Netherlands, **3** College of Agriculture, College of Animal Sciences, Yangtze University, Jingzhou, P. R. China, **4** Jiangsu Co-innovation Center for Prevention and Control of Important Animal Infectious Diseases and Zoonoses, Yangzhou University, Yangzhou, P. R. China

☯ These authors contributed equally to this work.
* liaoying@shvri.ac.cn

Citation: Gao B, Gong X, Fang S, Weng W, Wang H, Chu H, et al. (2021) Inhibition of anti-viral stress granule formation by coronavirus endoribonuclease nsp15 ensures efficient virus replication. PLoS Pathog 17(2): e1008690. https://doi.org/10.1371/journal.ppat.1008690

Editor: Volker Thiel, Universitat Bern, SWITZERLAND

Received: June 7, 2020

Accepted: February 1, 2021

Published: February 26, 2021

Peer Review History: PLOS recognizes the benefits of transparency in the peer review process; therefore, we enable the publication of all of the content of peer review and author responses alongside final, published articles. The editorial history of this article is available here: https://doi.org/10.1371/journal.ppat.1008690

Data Availability Statement: All relevant data are within the manuscript and its Supporting Information files.

Abstract

Cytoplasmic stress granules (SGs) are generally triggered by stress-induced translation arrest for storing mRNAs. Recently, it has been shown that SGs exert anti-viral functions due to their involvement in protein synthesis shut off and recruitment of innate immune signaling intermediates. The largest RNA viruses, coronaviruses, impose great threat to public safety and animal health; however, the significance of SGs in coronavirus infection is largely unknown. Infectious Bronchitis Virus (IBV) is the first identified coronavirus in 1930s and has been prevalent in poultry farm for many years. In this study, we provided evidence that IBV overcomes the host antiviral response by inhibiting SGs formation via the virus-encoded endoribonuclease nsp15. By immunofluorescence analysis, we observed that IBV infection not only did not trigger SGs formation in approximately 80% of the infected cells, but also impaired the formation of SGs triggered by heat shock, sodium arsenite, or NaCl stimuli. We further demonstrated that the intrinsic endoribonuclease activity of nsp15 was responsible for the interference of SGs formation. In fact, nsp15-defective recombinant IBV (rIBV-nsp15-H238A) greatly induced the formation of SGs, along with accumulation of dsRNA and activation of PKR, whereas wild type IBV failed to do so. Consequently, infection with rIBV-nsp15-H238A strongly triggered transcription of IFN-β which in turn greatly affected rIBV-nsp15-H238A replication. Further analysis showed that SGs function as an antiviral hub, as demonstrated by the attenuated IRF3-IFN response and increased production of IBV in SG-defective cells. Additional evidence includes the aggregation of pattern recognition receptors (PRRs) and signaling intermediates to the IBV-induced SGs. Collectively, our data demonstrate that the endoribonuclease nsp15 of IBV interferes with the formation of antiviral hub SGs by regulating the accumulation of viral dsRNA and by antagonizing the activation of PKR, eventually ensuring productive virus replication. We further demonstrated that nsp15s from PEDV, TGEV, SARS-CoV, and SARS-CoV-2 harbor the conserved function to interfere with the formation of chemically-induced SGs. Thus, we speculate that

Funding: This work was supported by the grant from the National Natural Science Foundation of China (No. 31772724) awarded to Y.L., the National Key Research and Development Program (No. 2017YFD0500802) awarded to Y.L., Elite Youth Program of Chinese Academy of Agricultural Sciences awarded to Y.L., the Central Public-interest Scientific Institution Basal Research Fund (2019JB03) awarded to Y.L., and National Natural Science Foundation of China (No. 31530074) awarded to C.D. The funders had no role in study design, data collection and analysis, decision to publish, or preparation of the manuscript.

Competing interests: The authors have declared that no competing interests exist.

coronaviruses employ similar nsp15-mediated mechanisms to antagonize the host anti-viral SGs formation to ensure efficient virus replication.

Author summary

Coronavirus encodes the conserved endoribonuclease nsp15, which has been reported to antagonize IFN responses by mediating evasion of recognition by dsRNA sensors. SGs are part of the host cell anti-viral response; not surprisingly, viruses in turn produce an array of antagonists to counteract such host response. Here, we show that IBV prevents the formation of SGs via nsp15, by reducing the accumulation of viral dsRNA, thereby evading the activation of PKR, phosphorylation of eIF2α, and formation of SGs. Depletion of SG scaffold proteins G3BP1/2 decreases IRF3-IFN response and increases the production of IBV. When overexpressed alone, nsp15s from different coronaviruses (IBV, PEDV, TGEV, SARS-CoV, and SARS-CoV-2) interferes with chemically- and physically-induced SGs, probably by targeting essential SGs assembly factors. In this way, coronaviruses antagonize the formation of SGs by nsp15, via reducing the viral dsRNA accumulation and sequestering/depleting critical component of SGs. To our knowledge, this is the first report describing the role of coronavirus nsp15 in the suppression of integral stress response, in crosstalk with anti-innate immune response.

Introduction

RNA viruses must generate double-stranded RNA (dsRNA) in order to replicate their genome. Host cells consequently employ a variety of pattern recognition receptors (PRRs) to detect dsRNA and trigger innate antiviral responses, which play a pivotal and critical role in fighting viral infections [1]. The host dsRNA-activated protein kinase R (PKR) is a key element of innate antiviral defenses [2]. Following binding to dsRNA, PKR undergoes auto-phosphorylation and phosphorylates the alpha subunit of eukaryotic initiation factor (eIF2α) on serine 51 [2,3]. Phospho-eIF2α tightly binds to eIF2B, prevents the recycling of ternary complex tRNA^{Met}-GTP-eIF2, and inhibits 43S translation complex formation, leading to global translation shut off, severely impairing virus replication [4]. In addition to PKR, there are three other eIF2α kinases involved in translation inhibition: PKR-like endoplasmic reticulum kinase (PERK), general control nonderepressible protein 2 (GCN2), and heme-regulated inhibitor kinase (HRI), which senses unfolded proteins in the endoplasmic reticulum (ER), nutrient starvation/ultraviolet radiation [5,6], and oxidative stress, respectively [7–9]. The translation inhibition leads to polysome disassembly and the subsequent assembly of stress granules (SGs), a membrane-less, highly dynamic warehouse for storing mRNA and translation components [10].

Environmental stressors triggering the translational inhibition and SG formation include ER stress, nutrient starvation, ultraviolet radiation, oxidative stress, heat shock, cold shock, proteasome inhibition, hyperosmotic stress, eIF4A inhibition, nitric oxide accumulation [11], perturbation of pre-mRNA splicing [12] and treatment with puromycin that results in disassembled polysomes [13]. SG formation is often downstream of the stress-activated phosphorylation of eIF2α, but some stressors trigger SG formation independently of eIF2α phosphorylation such as hyperosmotic stress and eIF4A inhibition. Once the protein translation is stopped, prion-like aggregation of Ras GTPase-activating protein-binding protein 1 (G3BP1),

T cell-restricted intracellular antigen 1 (TIA-1), and TIA-1-related protein (TIAR), promotes the formation of SGs, to store translation factors, mRNA, RNA binding proteins, and signaling proteins, etc [14–16]. Many RNA helicases were identified in SGs, such as RIG-I, DEAD/H-box helicases Ded1p/DDX3, eIF4A1, and RHAU [17,18]. RNA aggregation also plays a role in SG formation, which in turn, might be regulated by RNA helicases [19]. Thus, the abundance of mRNAs in the cytoplasm probably affects SGs formation. SGs not only protect mRNAs from harmful conditions, but also function as a decision point for untranslated mRNAs: storage, degradation, or re-initiation of translation [20]. Once stress is relieved and translation activities are restored, SGs are disassembled and mRNAs rapidly resume translation [21]. Although SGs can be generally induced through eIF2α-dependent or -independent pathways, during virus infections, SGs are mainly induced via the PKR-eIF2α pathway.

In addition to PKR, there are two other groups of PRRs to recognize dsRNA, namely Toll like receptors (TLRs) and RIG-I like receptors (RLRs) [22,23]. One of the TLRs, TLR3, located on the endosomal membrane, senses dsRNA and single stranded RNA (ssRNA) generated by RNA virus or DNA virus, in turn activates either the NF-κB or IRF3/7 pathway, resulting in boosting the production of proinflammatory cytokines and type I interferon (IFN) [24]. Another group of essential PRRs, RLRs, composed of RIG-I and MDA5, ubiquitously exist in the cytoplasm of mammalian cells, recognizes 5'-pppRNA and long dsRNA derived from RNA virus, respectively. Activation of RLRs by viral RNA leads to the aggregation of MAVS and recruitment of a series of signaling intermediates, transmits the signaling to transcription factor IRF3, IRF7, or NF-κB, eventually promoting the transcription of cytokines and type I IFN [25–27]. The secretion of type I IFN stimulates the transcription of IFN-stimulated genes (ISGs) via the JAK-STAT pathway, which protect neighboring cells from virus infection [28]. Recent evidence has shown that PKR and RLRs are localized to SGs during virus infection [29]. It is proposed that SGs exert specific antiviral activities by providing a platform for interaction between antiviral proteins and non-self RNA. To accomplish efficient replication, some viruses have evolved various mechanisms to circumvent the formation of anti-viral SGs. For instance, Influenza A Virus (IAV) NS1 protein and Vaccinia virus E3L sequester dsRNA from PKR [30,31], Ebola virus sequesters SG core proteins to viral inclusion body [32], thereby inhibiting the formation of SGs. For some picornaviruses, leader protease and 3C protease of Foot-and-Mouth Disease Virus (FMDV) and 2A protease of Enterovirus 71, disassemble the SGs by cleaving G3BP1 or G3BP2 [33–36]. As for coronaviruses, recent studies show that Middle East Respiratory Syndrome Coronavirus (MERS-CoV) 4a accessory protein limits the activation of PKR by binding to dsRNA, thereby inhibiting the formation of SGs and ensuring viral protein translation and efficient virus replication [37,38]. Mouse Hepatitis Virus (MHV) replication induces host translational shutoff and mRNA decay, with concomitant formation of SGs and processing bodies [39]. Porcine Transmissible Gastroenteritis Virus (TGEV) induced SG like granules correlated with viral replication and transcription [40]. In the context of MHV or TGEV infection, the percentage of SGs positive cells to infected cells has not shown. Severe Acute Respiratory Syndrome *Coronavirus* (SARS-CoV), SARS-CoV-2 and IBV N proteins have been found to interact with the key SG component G3BP1 [41,42]. A recent report shows that infectious bronchitis virus (IBV) infection results in the formation of SGs in approximately 20% of infected cells and inhibits eIF2α-dependent and -independent SG formation by unknown mechanisms [43].

Coronaviruses harbor the largest positive-stranded RNA genome among the RNA viruses, with size from 27 kb to 32 kb. The two-third of the 5' terminus encodes replicase polyproteins (1a and 1ab), while one-third of the 3' terminus encodes spike protein (S), envelope protein (E), membrane protein (M), nucleocapsid protein (N) and accessory proteins. The proteolysis of overlapped polyproteins is processed by two self-encoded proteases, papain-like protease

(PLpro) and 3C-like protease (3CLpro), into 15–16 mature non-structural proteins (nsp1-nsp16). Most of the nsps assemble into a replication and transcription complex (RTC) responsible for virus replication, while several nsps mediate the evasion of host innate immune responses. For example, severe acute respiratory syndrome coronavirus (SARS-CoV) and MERS-CoV nsp1 suppresses host gene expression by mediating host mRNA degradation [44]; the PLpro nsp3 of SARS-CoV and MERS-CoV harbors deubiquitinase activity and interferes with type I IFN responses [45,46]; Feline Infectious Peritonitis Coronavirus (FCoV) and Porcine *Delta*-coronavirus (PDCoV) nsp5 inhibits type I IFN response by cleaving NEMO [47,48]; porcine epidemic diarrhea virus (PEDV) nsp16 restricts IFN production and facilitate virus replication [49]. Nsp15 is a conserved poly(U) specific endoribonuclease in coronavirus and have been demonstrated to be a new member on the list of IFN antagonists [50]. It has been demonstrated that MHV and HCoV-229E nsp15 endoribonuclease activity is key to evade dsRNA sensing by host sensors and to ensure efficient coronavirus replication [51,52]. PEDV nsp15 endoribonuclease activity is important for suppressing type I and type III IFN responses and to facilitate replication, shedding, and pathogenesis [53]. However, whether IBV nsp15 is involved in antagonizing to host anti-viral response, has not been determined yet.

IBV is the first identified coronavirus in 1930s and infects avian species, belonging to *gamma*-coronavirus [54]. It causes a prevalent disease that has led to substantial economic losses in poultry farm for many decades. Elucidating host responses to virus infections is fundamental to understand virus replication and to identify targets for therapeutic control. In this study, we infected three types of cells with IBV, and found that approximately 80% of infected cells did not display SGs formation. IBV also hindered SGs formation triggered by different stimuli. Further analysis showed that IBV nsp15 was involved in the inhibition of SG formation, and that the endoribonuclease activity of nsp15 particularly played a pivotal role. Compared to wild type IBV, infection with the nsp15 endoribonuclease catalytic deficient mutant, rIBV-nsp15-H238A, led to accumulation of higher levels of dsRNA, strong activation of PKR, more SGs formation, concomitantly with a higher production of IFN-β and lower viral replication. Furthermore, we used SG-defective cells to demonstrate that SGs play an anti-viral role by promoting the IFN response. Moreover, the anti-SG formation by nsp15 is conserved in different genera of coronaviruses.

Results

IBV does not trigger SGs formation in the majority of infected cells

In this study, we mainly used the IBV-Beaudette strain to study the host stress response to coronavirus infection. To facilitate the detection of cellular proteins, and due to the unavailability of antibodies against chicken proteins of interest (see S1 Table), we used mammalian H1299 (IFN competent) and Vero (IFN deficient) cell lines, which are permissive to the IBV-Beaudette strain, in addition to chicken fibroblast DF-1 cells. To determine whether IBV replication induces SGs formation, cells were infected with IBV at MOI = 1. The occurrence of SGs was assessed by visualizing G3BP1 granules formation while IBV infection was monitored by visualizing the N protein. We determined the kinetics of SGs formation upon infection at 4 hours intervals, by counting the cells with IBV-N protein expression and by calculating the proportion of these that was also positive for G3BP1 granules. In all the three cell types, despite efficient virus infection, as indicated by the expression of N protein and syncytia formation, no SGs formation could be detected from 0 to 8 hours post-infection (h.p.i.), whereas from 12 to 24 h.p.i., G3BP1 granules could be detected, but only in approximately 5%-25% of infected cells (Fig 1A–1C). These observations indicate that IBV cannot effectively trigger SGs formation in most infected cells. In SGs positive cells, another SGs marker, TIAR, was found to colocalize with G3BP1 granules, demonstrating that IBV induces canonical SGs (Fig 1D and 1E).

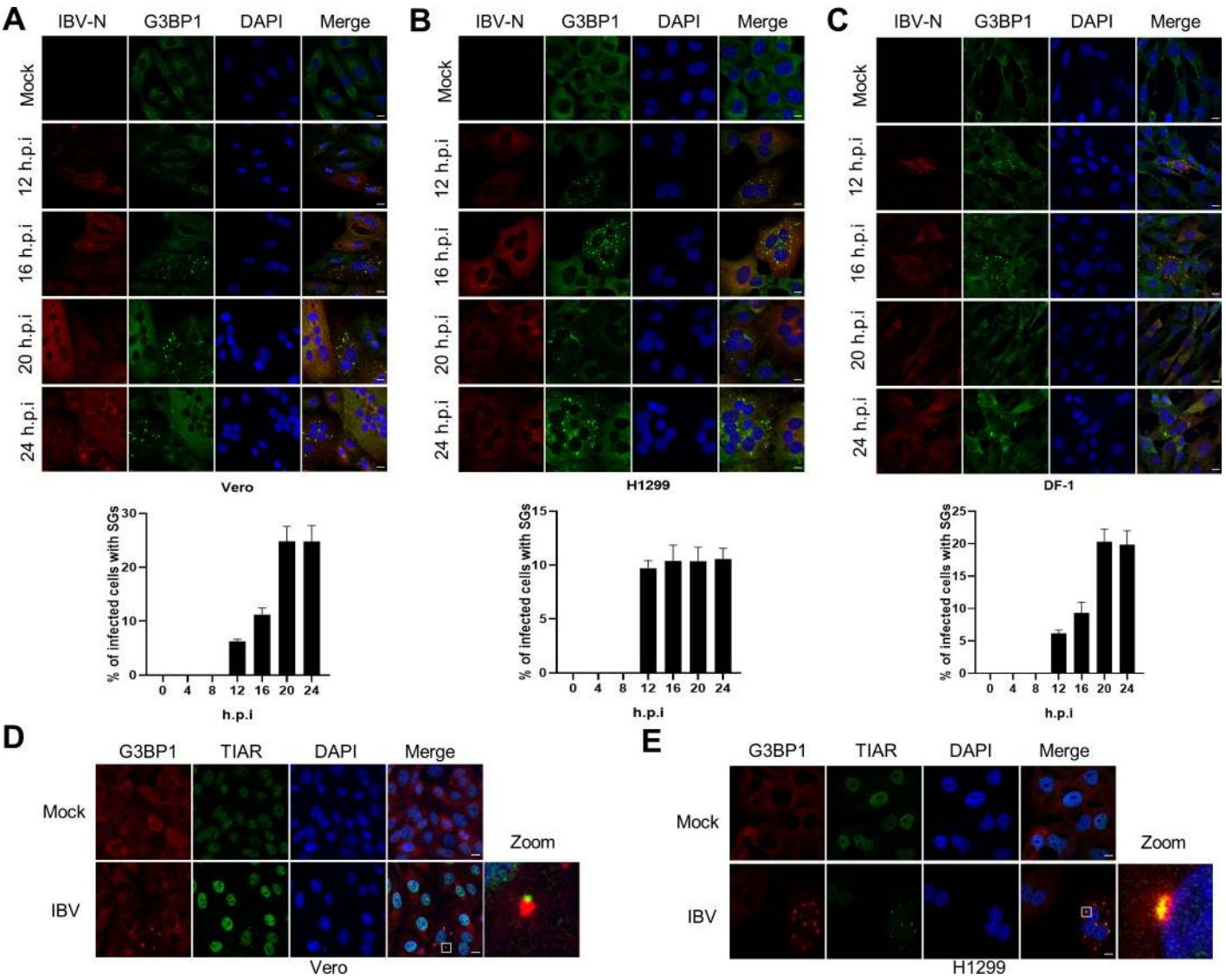

Fig 1. IBV prevents SGs formation in the majority of infected cells. (A-C) Vero, H1299, and DF-1 cells were infected with IBV Beaudette strain at an MOI of 1 or mock infected. At the indicated time points, cells were subjected to immunostaining. Infected cells (red) were identified using a rabbit anti-N protein, SGs (green) with a (cross-reacting) mouse anti-G3BP1 and cell nuclei with DAPI (blue). The bar graphs showed the percentage of SGs positive cells to infected cells, which was counted in 20 random fields, presented as mean ± SD. (D and E) Vero and H1299 cells were infected with IBV as described in A-C. At 20 h.p.i., immunostaining was used to visualize the position of the structural components of SGs using anti-G3BP1 (red) and anti-TIAR (green) antibodies. The enlargement of the insets confirms their co-localization in cytoplasmic granules. The representative images of three independent experiments were shown. Scale bars: 10 μm.

https://doi.org/10.1371/journal.ppat.1008690.g001

To convincingly demonstrate that these foci are genuine SGs, not RNP or RNA granules, IBV-infected cells were treated with cycloheximide (CHX) to trap mRNAs at polysomes and prevent SG assembly. As shown in S1 Fig, CHX treatment dissolved the IBV-triggered SGs: the SG positive cells decreased from approximately 12% to 2% in H1299 and from 19% to 5% in DF-1. Thus, the G3BP1 foci represent genuine SGs.

Phosphorylation status of PKR and eIF2α during IBV infection

Several past studies demonstrated that some viruses impede SGs formation by preventing the activation of PKR, or by cleaving the SG scaffold protein G3BP1 [55,56]. To elucidate the

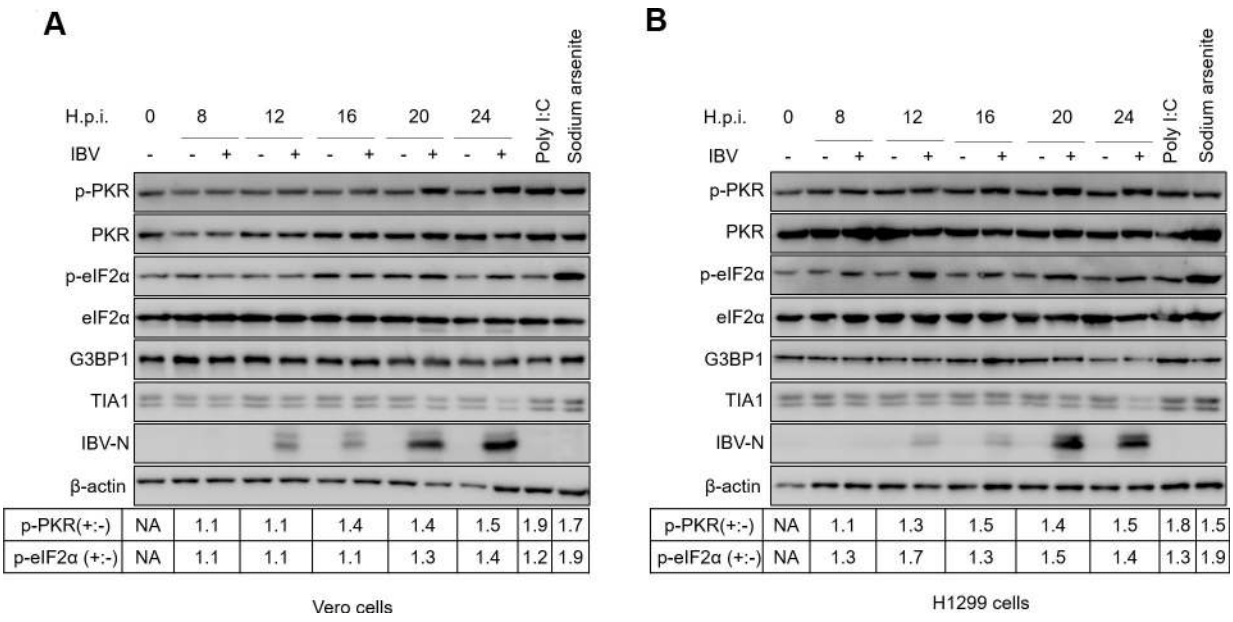

Fig 2. PKR and eIF2α phosphorylation status during IBV infection. (A and B) Vero and H1299 cells were infected with IBV at a MOI of 1. Mock infection was included as negative control, poly I:C transfection for 6 h or 1 mM sodium arsenite for 30 min were included as positive control. Cells were harvested at the indicated time points and processed for western blot analysis using 10 μg total protein per lane. p-PKR, PKR, p-eIF2α, eIF2α, G3BP1, TIA-1, and IBV-N were detected with corresponding antibodies. β-actin was probed as a loading control. The representative images of two independent experiments were shown. The signals of protein bands were determined by Image J. The intensities of p-PKR or p-eIF2α were normalized to total PKR or total eIF2α. The ratio of p-PKR and p-eIF2α in IBV-infected cells, poly I:C-transfected cells, or sodium arsenite-treated cells, to mock-infected cells, were shown as p-PKR (+:-) or p-eIF2α (+:-).

https://doi.org/10.1371/journal.ppat.1008690.g002

inhibition mechanisms of SG formation by IBV, we investigate whether IBV interferes with the phosphorylation of PKR and eIF2α, or directly affects TIA-1 and G3BP1 protein levels. After having assessed that IBV prevents SGs formation not only in chicken cells but also in mammalian cells, due to the availability of antibodies directed against mammalian proteins and their lack of cross-reactivity to the chicken proteins of interest, we next proceeded with Vero and H1299 cells. Poly I:C transfection or sodium arsenite treatment were included as positive control to stimulate phosphorylation of PKR and eIF2α [57]. As shown in Fig 2A and 2B, compared to mock-infected cells, the level of phospho-PKR was gradually increased along with the infection time course, peaked at 20 and 24 h.p.i., which was lower than those in poly I:C-transfected or sodium arsenite-treated cells. Accordingly, a slight increase of phospho-eIF2α was observed in IBV-infected cells, which was lower than that in sodium arsenite-treated cells. It was noted that poly I:C transfection greatly stimulated phosphorylation of PKR, but not phosphorylation of eIF2α, and the underlying mechanism is unclear. In parallel, we did not observe any cleavage product of either G3BP1 or TIA-1 throughout IBV infection in both H1299 and Vero cells. Combined with the above results showing that approximately 20% of infected cells displayed SGs formation (Fig 1), these results imply that IBV activates PKR in a small proportion of infected cells, which contributes to SGs formation; in the majority of infected cells however, IBV evades PKR recognition and avoids triggering SGs formation.

IBV blocks both eIF2α-dependent and -independent SGs formation

During the course of our study, it was reported that IBV inhibits eIF2α-dependent and -independent SGs induction in Vero cells [43]. Here, we used H1299 and DF-1 cells to further

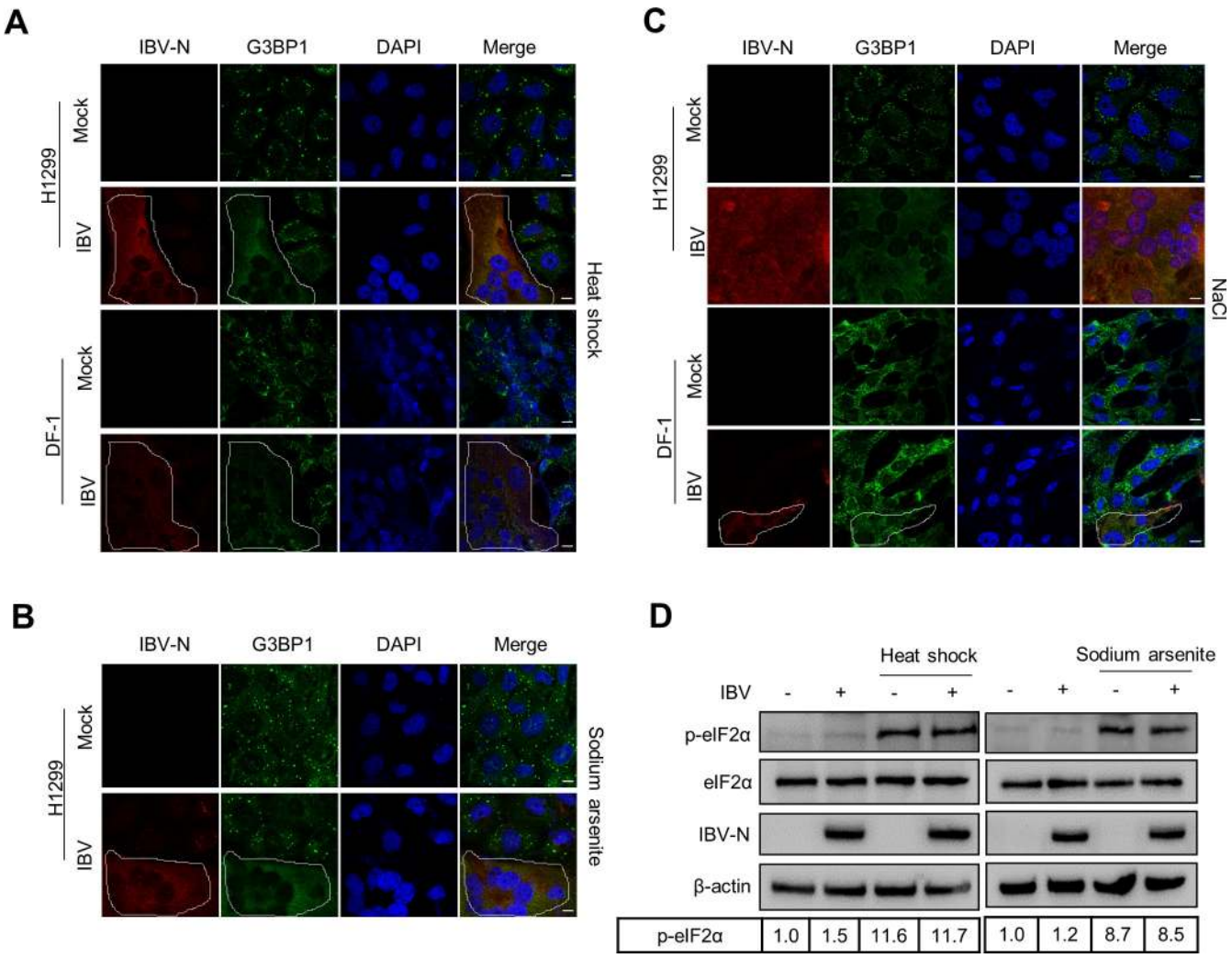

Fig 3. IBV abrogates eIF2α-dependent and -independent formation of SGs. (A-C) H1299 and DF-1 cells were infected with IBV an MOI of 1. At 20 h.p.i., cells received heat shock treatment (50˚C for 20 min), 1 mM sodium arsenite for 30 min, or 200 mM NaCl for 50 min, followed by immunostaining. Infected cells were detected with anti-N antibody (red), SGs with anti-G3BP1 (green) and cell nuclei with DAPI (blue). The representative images of three independent experiments were shown. Scale bars: 10 μm. (D) H1299 cells were mock-infected or infected with IBV and treated with heat shock or sodium arsenite as described in A and B. At 20 h.p.i., cell lysates (10 μg per lane) were subjected to western blotting analysis to detect p-eIF2α, eIF2α, IBV-N, and β-actin. The representative data of three independent experiments were shown. The signals of protein bands were determined by Image J. The intensities of p-eIF2α were normalized to total eIF2α. The ratio of p-eIF2α in IBV-infected cells, heat shock-treated cells, or sodium arsenite-treated cells, to mock-infected cells, were shown as p-eIF2α.

https://doi.org/10.1371/journal.ppat.1008690.g003

investigate the inhibition of SGs by IBV. H1299 and DF-1 cells were infected with IBV and treated with three different stress stimuli (sodium arsenite, heat shock and NaCl) to induce SGs formation. Sodium arsenite or heat shock promote phosphorylation of eIF2α in PKR- or HRI kinase-dependent manner, leading to translational arrest and subsequent formation of SGs [57,58], whereas NaCl may enhance the local concentration of mRNAs and cellular proteins by decreasing the cell volume, thereby inducing SGs in an eIF2α-independent manner [59]. In non-infected cells, more than 90% of cells were positive for SGs formation after treatment with these stress stimuli; interestingly, IBV infection prevented SGs formation triggered by these stimuli, as evidenced by the absence of G3BP1 granules exclusively in IBV-positive cells (Fig 3A–3C). Unfortunately, sodium arsenite treatment inefficiently triggered G3BP1 aggregation in DF-1 cells due to unknown reasons. These results indicate that IBV infection

blocks both eIF2α-dependent and -independent SGs formation in mammalian and avian cells. We next explore whether IBV interferes with the phosphorylation of eIF2α triggered by sodium arsenite or heat shock. We observed a significant upregulation of phospho-eIF2α by sodium arsenite or heat shock treatment in H1299 cells; however, there was no reduction of phospho-eIF2α by IBV infection (Fig 3D). Collectively, these data indicate that IBV infection restricts both eIF2α-dependent and -independent SGs formation, probably by interfering with SG assembly or disassembly and not with inhibition of eIF2α phosphorylation.

IBV endoribonuclease nsp15 is responsible for prevention of SGs formation

To screen the IBV proteins involved in prevention of SGs formation, we expressed individual Flag-tagged IBV protein in H1299 cells and triggered the formation of SGs with heat shock. The schematic diagram of proteins encoded by IBV is shown in Fig 4A. In cells expressing nsp2, nsp4, nsp5, nsp6, nsp7, nsp8, nsp9, nsp12, nsp16, 3b, E, 5a, 5b, M, or N, SGs formation remained intact (Fig 4B), suggesting that alone these proteins have no inhibitory effect on the formation of SGs. Interestingly, only in nsp15-expressing cells, the heat shock-induced SGs were absent (as indicated by white arrow), suggesting that nsp15 may be the viral protein responsible for efficient suppression of SGs formation. We also investigated, but failed to detect, the expression of nsp3, nsp10, nsp13, nsp14, S, and 3a, therefore it cannot be excluded that also these viral proteins might be involved in inhibition of SGs formation. These results however demonstrate that nsp15 alone is sufficient to block SGs formation.

Nsp15 is a conserved endoribonuclease of coronaviruses. It has been reported that its activity is involved in evasion of dsRNA sensing and interference with the type I IFN response [51,52]. The conserved histidine (H) 223 and H238 of IBV nsp15 are critical for the endoribonuclease activity [50]. To examine whether the endoribonuclease activity is involved in prevention of SGs formation, we introduced an alanine (A) substitution in the catalytic core residues H223 or H238, to abrogate the catalytic activity. We next compared the ability of wild type nsp15, nsp15-H223A, and nsp15-H238A to prevent SGs formation in H1299 cells. As expected, wild type nsp15 interfered with the formation of SGs induced by heat shock, sodium arsenite, or NaCl (indicated with white arrow), while nsp15-H223A and nsp15-H238A did not (Fig 5A–5C). Thus, the nsp15 endoribonuclease activity is required for the inhibition of eIF2α-dependent and -independent SGs formation.

In a preliminary investigation of how nsp15 may prevent SGs formation, we examined whether nsp15 interferes with the phosphorylation of eIF2α. We observed a significant increase of phospho-eIF2α by sodium arsenite or heat shock treatment (Fig 5D); however, in agreement with the data on IBV-infected cells (Fig 3D), no reduction of phospho-eIF2α was observed in nsp15-expressing cells (Fig 5D). No difference was observed in the protein levels of G3BP1 and TIA-1 in nsp15-expressing cells, compared to control cells. Taken together, these data indicate that nsp15 interferes with the formation of SGs, downstream of eIF2α.

The anti-SG formation function of nsp15 is conserved in different genera of coronaviruses

Since nsp15 is highly conserved in catalytic core domains across all coronaviruses (S2 Fig), we sought to determine whether the anti-SG formation we detected in IBV nsp15 is conserved in other coronaviruses. There are two conserved histidine critical for the endoribonuclease activity in the core domain in all nsp15s from different coronaviruses (S2 Fig). Flag-tagged nsp15 and the endonuclease catalytic activity deficient mutants (H-A) from alpha-coronavirus PEDV and TGEV, beta-coronavirus SARS-CoV and SARS-CoV-2 were expressed alone in corresponding host cells (LLC-PK1, ST, or HeLa cells), followed by sodium arsenite or NaCl

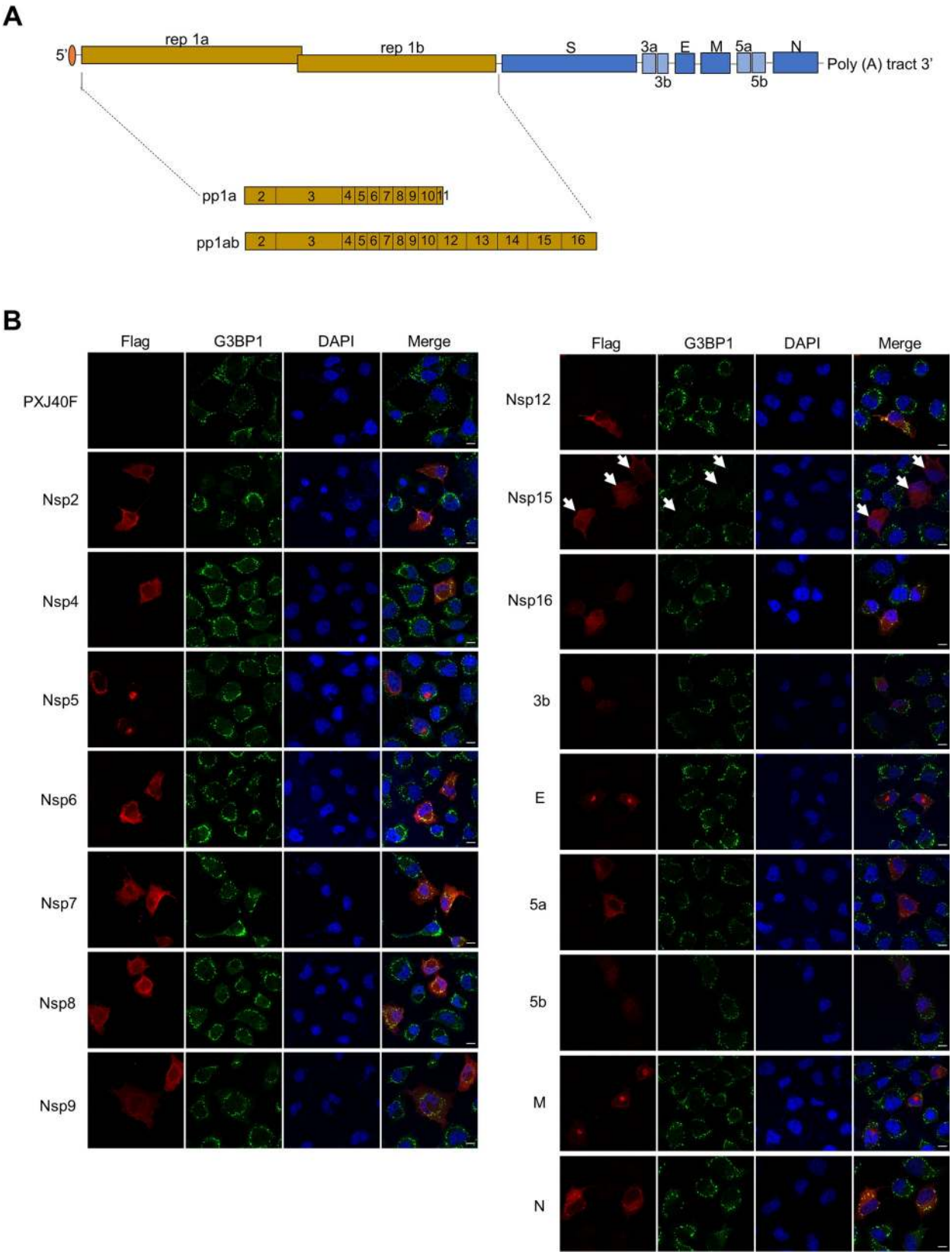
A
5'
rep 1a
rep 1b
S
3a
E
M
5a
N
Poly (A) tract 3'
3b
5b
pp1a
2 3 4 5 6 7 8 9 10 11
pp1ab
2 3 4 5 6 7 8 9 10 12 13 14 15 16
B
Flag
G3BP1
DAPI
Merge
PXJ40F
Nsp2
Nsp4
Nsp5
Nsp6
Nsp7
Nsp8
Nsp9
Nsp12
Nsp15
Nsp16
3b
E
5a
5b
M
N

Fig 4. IBV nsp15 inhibits the formation of SGs. (A) Schematic diagram of the proteins encoded by IBV. (B) H1299 cells were transfected with plasmids encoding Flag-tagged IBV proteins or with vector PXJ40F. At 24 h post-transfection, cells received heat shock treatment at 50˚C for 20 min. IBV proteins were stained with anti-Flag antibody (red) and SGs were detected with anti-G3BP1 (green). Cell nuclei were stained with DAPI (blue). The representative images of three independent experiments were shown. Scale bars: 10 μm.

https://doi.org/10.1371/journal.ppat.1008690.g004

treatment. As expected, wild type nsp15 from different coronaviruses prevented the formation of SGs induced by sodium arsenite or NaCl (Fig 6A–6D), while nsp15 endonuclease catalytic activity deficient mutants did not (Fig 6A–6D). Thus, the ability of nsp15 endonuclease to prevent SG formation is conserved in different genera of coronaviruses.

Overexpression of coronavirus nsp15 induces PABP1 nuclear localization

Poly(A)-binding protein 1 (PABP1) has a fundamental role in the regulation of mRNA translation and stability. Although generally a diffuse cytoplasmic protein, in conditions of cell stress, PABP1 is incorporated into cytoplasmic SGs [60]. Since coronavirus nsp15 prevents SG formation, we examined whether nsp15 interferes with the incorporation of PABP1 into SGs. We expressed Flag-tagged nsp15 and the endonuclease catalytic activity deficient mutants (H-A) from IBV, PEDV, TGEV, SARS-CoV, SARS-CoV-2 in H1299, LLC-PK1, ST, or HeLa cells, respectively, followed by heat shock treatment or sodium arsenite treatment. Immunofluorescence results showed that heat shock or sodium arsenite induced discrete cytoplasmic foci of PABP1, suggesting the incorporation PABP1 into SGs (Fig 7A–7E); however, in nsp15 overexpressing cells, PABP1 located to nucleus, while the endoribonuclease deficient mutants (H-A) did not (Fig 7A–7E). These results indicate that nsp15 is involved in PABP1 nuclear localization. Considering that nsp15 endonuclease activity is required for PABP1 nuclear localization, nsp15 might target host cell RNA to relocate PABP1 to the nucleus.

Nsp15-defective recombinant virus rIBV-nsp15-H238A induces canonical SGs by accumulation of dsRNA and activation of PKR

To further confirm the involvement of the endoribonuclease activity of nsp15 in the prevention of SGs formation, we constructed nsp15-defective recombinant virus rIBV-nsp15-H238A in which the nsp15 catalytic site H238 was replaced with an alanine (Fig 8A). We also constructed, but failed to recover nsp15-defective rIBV-nsp15-H223A, possibly due to the effect of the disruption of the catalytic site on virus replication. Firstly, we compared the replication dynamics of wild type IBV and rIBV-nsp15-H238A in Vero, H1299, and DF-1 cells by $TCID_{50}$ assay. As shown in Fig 8A, in IFN competent H1299 and DF-1 cells, the replication of rIBV-nsp15-H238A was significantly lower than that of wild type IBV, suggesting that the endonuclease activity of nsp15 is required for efficient virus replication; however, in IFN deficient Vero cells [61], the replication of rIBV-nsp15-H238A was partially restored. Considering that Vero cells are IFN deficient [61], we speculate that the IFN response in H1299 and DF-1 cells might be responsible for impaired rIBV-nsp15-H238A replication. rIBV-nsp15-H238A replication however, was not fully restored in Vero cells, indicating that other factors may contribute to the attenuation of this nsp15-defective virus.

Next, we compared the ability of wild type IBV and rIBV-nsp15-H238A to induce the formation of SGs in Vero, H1299 and DF-1 cells. At 20 h.p.i., only 24% of Vero cells, 18% of H1299 cells, and 17% of DF-1 cells infected with wild type IBV showed the presence of SGs, whereas approximately 43% of the Vero cells, 78% of the H1299 cells, and 75% of DF-1 cells infected with rIBV-nsp15-H238A showed the presence of SGs (Fig 8B). The percentage of SGs positive cells in rIBV-nsp15-H238A-infected Vero cells was lower than in H1299 or DF-1 cells infected with the same virus, suggesting that the IFN response is probably involved in

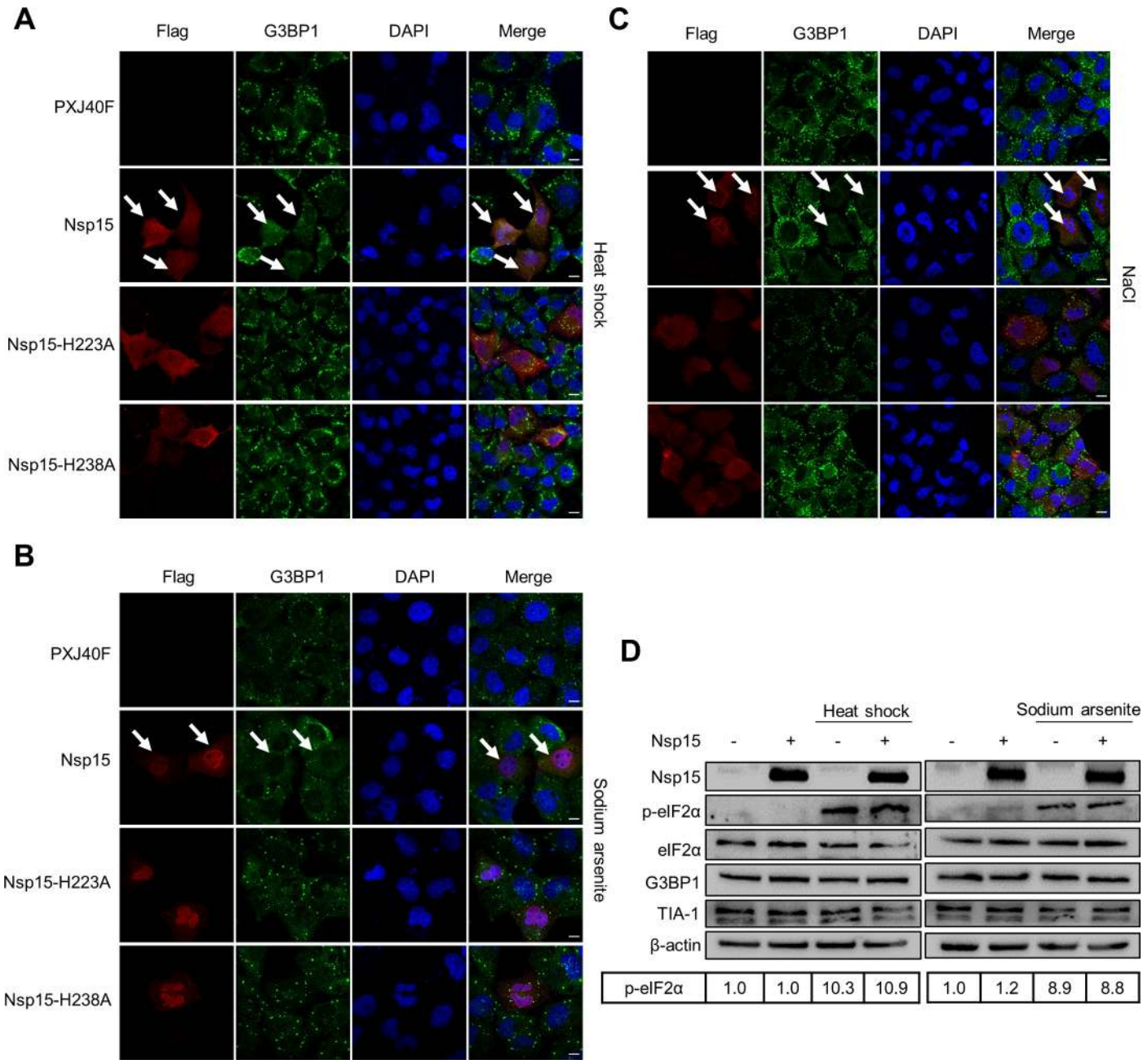

Fig 5. IBV nsp15 endoribonuclease activity is required for inhibition of eIF2α-dependent and -independent formation of SGs. (A-C) H1299 cells were transfected with plasmids encoding IBV nsp15, nsp15-H223A, or nsp15-H238A, respectively. At 24 h post-transfection, cells received heat shock, sodium arsenite, or NaCl treatment. Nsp15, nsp15-H223A, and nsp15-H238A were detected with anti-Flag antibody (red) and G3BP1 was detected with anti-G3BP1 (green). Cell nuclei were stained with DAPI (blue). The representative images of three independent experiments were shown. Scale bars: 10 μm. (D) H1299 cells were transfected with plasmids encoding IBV nsp15 or with vector PXJ40F. At 24 h post-transfection, cells received heat shock or sodium arsenite treatment. Cell lysates (10 μg/lane) were subjected to Western blot analysis, to check the expression of Flag-nsp15 and to determine the levels of phospho-eIF2α, eIF2α, G3BP1, TIA-1, and β-actin. The representative data of two independent experiments were shown. The signals of protein bands were determined by Image J. The intensities of p-eIF2α were normalized to total eIF2α. The ratio of p-eIF2α in nsp15-transfected cells, heat shock-treated cells, soduim arsenite-treated cells, to vector PXJ40F-transfected cell, were shown as p-eIF2α.

https://doi.org/10.1371/journal.ppat.1008690.g005

promoting the formation of SGs. Treatment with cycloheximide dissolved the rIBV-nsp15-H238A-induced G3BP1 and G3BP2 granules (Fig 8C), confirming that rIBV-nsp15-H238A induces canonical SGs. SG assembly occurs in a multistep fashion and recent evidence points

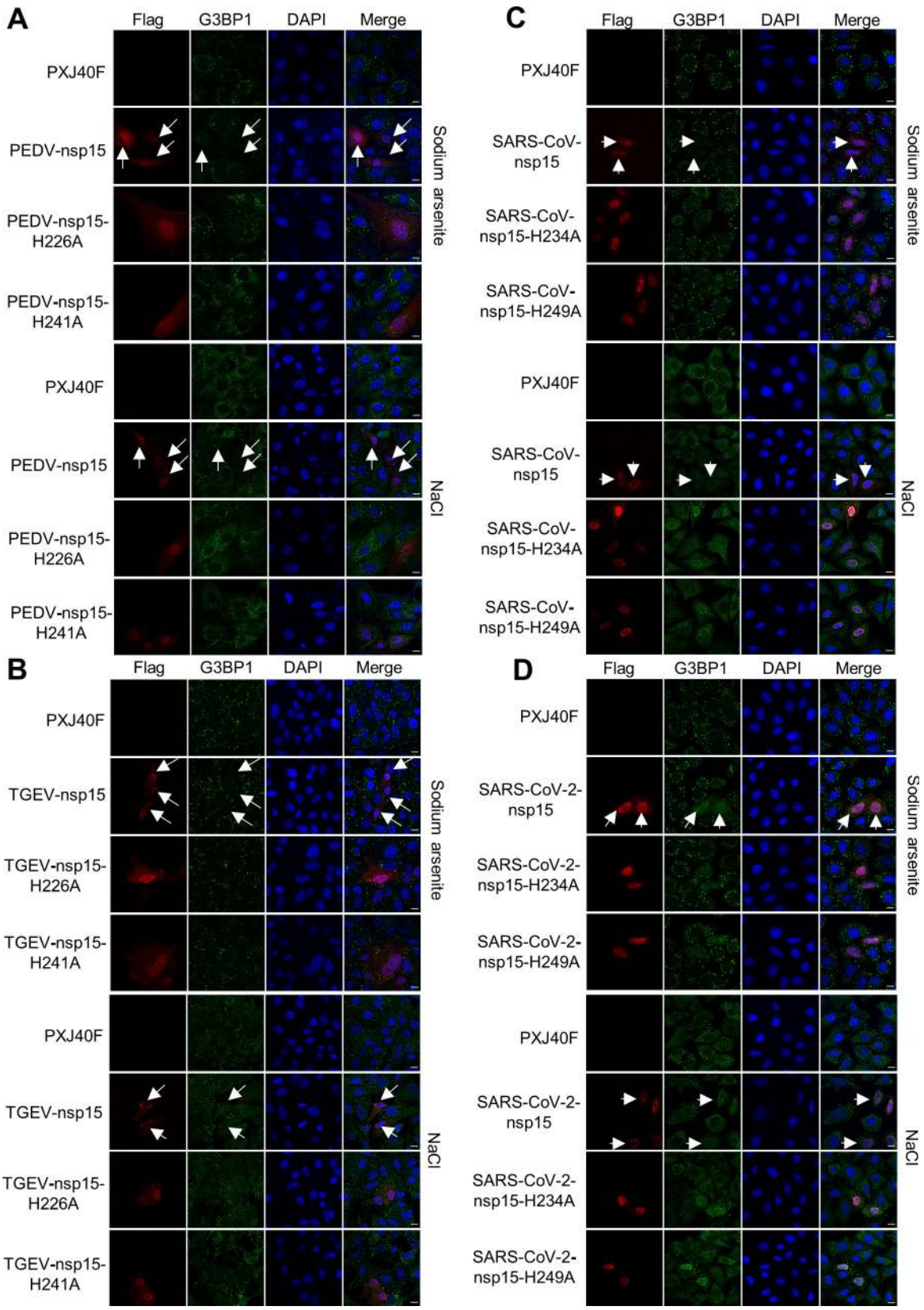
A
Flag
G3BP1
DAPI
Merge
PXJ40F
PEDV-nsp15
PEDV-nsp15-H226A
PEDV-nsp15-H241A
PXJ40F
PEDV-nsp15
PEDV-nsp15-H226A
PEDV-nsp15-H241A
Sodium arsenite
NaCl
B
Flag
G3BP1
DAPI
Merge
PXJ40F
TGEV-nsp15
TGEV-nsp15-H226A
TGEV-nsp15-H241A
PXJ40F
TGEV-nsp15
TGEV-nsp15-H226A
TGEV-nsp15-H241A
Sodium arsenite
NaCl
C
Flag
G3BP1
DAPI
Merge
PXJ40F
SARS-CoV-nsp15
SARS-CoV-nsp15-H234A
SARS-CoV-nsp15-H249A
PXJ40F
SARS-CoV-nsp15
SARS-CoV-nsp15-H234A
SARS-CoV-nsp15-H249A
Sodium arsenite
NaCl
D
Flag
G3BP1
DAPI
Merge
PXJ40F
SARS-CoV-2-nsp15
SARS-CoV-2-nsp15-H234A
SARS-CoV-2-nsp15-H249A
PXJ40F
SARS-CoV-2-nsp15
SARS-CoV-2-nsp15-H234A
SARS-CoV-2-nsp15-H249A
Sodium arsenite
NaCl

Fig 6. Nsp15s from PEDV, TGEV, SARS-CoV, SARS-CoV-2 harbor the conserved function to inhibit eIF2α-dependent and -independent formation of SGs, and the endoribonuclease activity is required. LLC-PK1, ST or HeLa cells were transfected with plasmids encoding Flag-tagged nsp15s or their catalytic defective mutants (H-A) from PEDV (LLC-PK1 cells), TGEV (ST cells), SARS-CoV (HeLa cells), SARS-CoV-2 (Hela cells), respectively. At 24 h post-transfection, cells were received sodium arsenite or NaCl treatment. The cells expressing Flag-tagged nsp15s or catalytic defective mutants were detected with anti-Flag antibody (red) and the formation of SGs was detected with anti-G3BP1 (green). Cell nuclei were stained with DAPI (blue). The representative images of three independent experiments were shown. Scale bars: 10 μm.

https://doi.org/10.1371/journal.ppat.1008690.g006

towards the accumulation of UBAP2L foci seeding larger G3BP1 positive granules [62]. Results in S3 Fig showed that either sodium arsenite stimulation or rIBV-nsp15-H238A infection triggered UBAP2L foci, well co-localized with G3BP1, further demonstrating that rIBV-nsp15-H238A induces genuine SGs.

In agreement, infection of H1299 cells with rIBV-nsp15-H238A significantly activated PKR by phosphorylation and in turn phosphorylated eIF2α, while wild type IBV did not (Fig 9A). Thus, nsp15 endoribonuclease activity is involved in antagonizing PKR activation, the well characterized dsRNA sensor and IFN-β inducer. Again, Western blot showed that the replication of rIBV-nsp15-H238A was impaired, as evidenced by the decreased level of IBV-S, IBV-M, and IBV-N protein synthesis, compared to wild type IBV (Fig 9A). Upon infected with rIBV-nsp15-H238A, it was noted that in IFN deficient Vero cells, activation of PKR and phosphorylation of eIF2α was not as obvious as that in H1299 cells, although replication of rIBV-nsp15-H238A was comparable to that of wild type IBV (S4 Fig). This is consistent with the data showing a lower percentage of SGs positive cells in rIBV-nsp15-H238A-infected Vero cells than in H1299 and DF-1 cells (Fig 8B). Although rIBV-nsp15-H238A replication was low in H1299 and DF-1 cells, it significantly stimulated the transcription of IFN-β at 20 h.p.i., which was approximately 25-fold higher than that induced by wild type IBV in H1299 cells (Fig 9B, left panel), and approximately 380-fold higher than that induced by wild type IBV in DF-1 cells (Fig 9B, right panel). Taken together, the activation of PKR by rIBV-nsp15-H238A and associated induction of type I IFN might be responsible for the lower replication of this recombinant virus.

The activation of PKR by rIBV-nsp15-H238A prompted us to measure and compare the levels of dsRNA during infection by using the specific J2 monoclonal antibody, which binds dsRNA greater than 40 nucleotides in length [50] and was previously successfully used during IBV infection in chicken cells [63]. Immunofluorescence analysis at 20 h.p.i., revealed evident higher accumulation of dsRNA in rIBV-nsp15-H238A-infected H1299 cells when compared to wild type IBV-infected cells (Fig 9C). The dsRNA produced by rIBV-nsp15-H238A however, did not colocalized with G3BP1 granules, suggesting that the dsRNA is not recruited to SGs (Fig 9C). DsRNA dot blot analysis also supported the observation that infection with rIBV-nsp15-H238A leads to higher accumulation of dsRNA than infection with wild type IBV in both H1299 and DF-1 cells (Fig 9D). We speculated that when compared to wild type IBV, rIBV-nsp15-H238A replication leads to higher accumulation of dsRNA and that the excess dsRNA may escape from replication-transcription complex (RTC). The "free" dsRNA in turn, triggers the activation of PKR and phosphorylation of eIF2α resulting in translational shut off, eventually promoting the formation of SGs and activation of the type I IFN response. RT-PCR examination of the level of viral RNA showed that infection with rIBV-nsp15-H238A indeed led to an increased ratio of negative strand RNA:positive strand RNA, compared to infection with wild type IBV (S5 Fig). This suggests that functional nsp15 is required for maintaining the ratio of viral (-: +) RNA, probably by reducing the abundance of negative strand RNA. Altogether, these data indicate that intact nsp15 endoribonuclease activity acts to reduce the intracellular levels of dsRNA, thereby preventing activation of PKR and SGs formation.

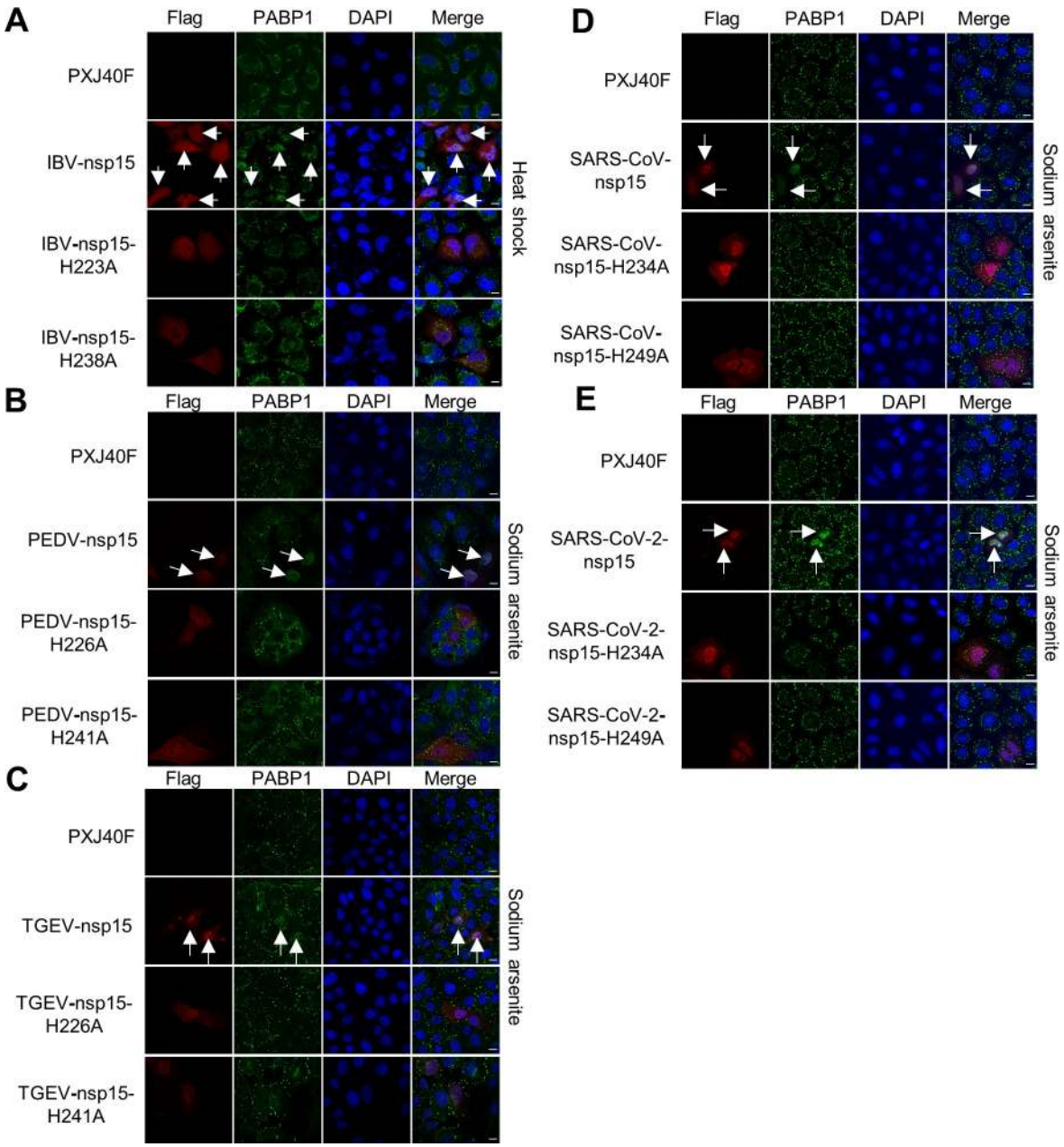

Fig 7. Nsp15s from IBV, PEDV, TGEV, SARS-CoV, SARS-CoV-2 harbor the conserved function to retain PABP1 in nucleus and endoribonuclease activity is required. H1299, LLC-PK1, ST or HeLa cells were transfected with plasmids encoding Flag-tagged nsp15s or their catalytic defective mutants (H-A) from IBV (H1299 cells), PEDV (LLC-PK1 cells), TGEV (ST cells), SARS-CoV (HeLa cells), SARS-CoV-2 (Hela cells), respectively. At 24 h post-transfection, cells were received heat shock or sodium arsenite treatment. The cells expressing Flag-tagged nsp15s or catalytic defective mutants were detected with anti-Flag antibody (red) and PABP1 was detected with anti-PABP1 (green). Cell nuclei were stained with DAPI (blue). The representative images of three independent experiments were shown. Scale bars: 10 μm.

https://doi.org/10.1371/journal.ppat.1008690.g007

Nsp15-defective rIBV-nsp15-H238A strongly activates the IRF3-IFN signaling via the formation of SG

To examine the role of SGs in IBV infection, we knocked out the SGs core protein G3BP1 and G3BP2 in H1299 cells by a CRISPR-Cas9 approach. Depletion of G3BP1/2 resulted in the

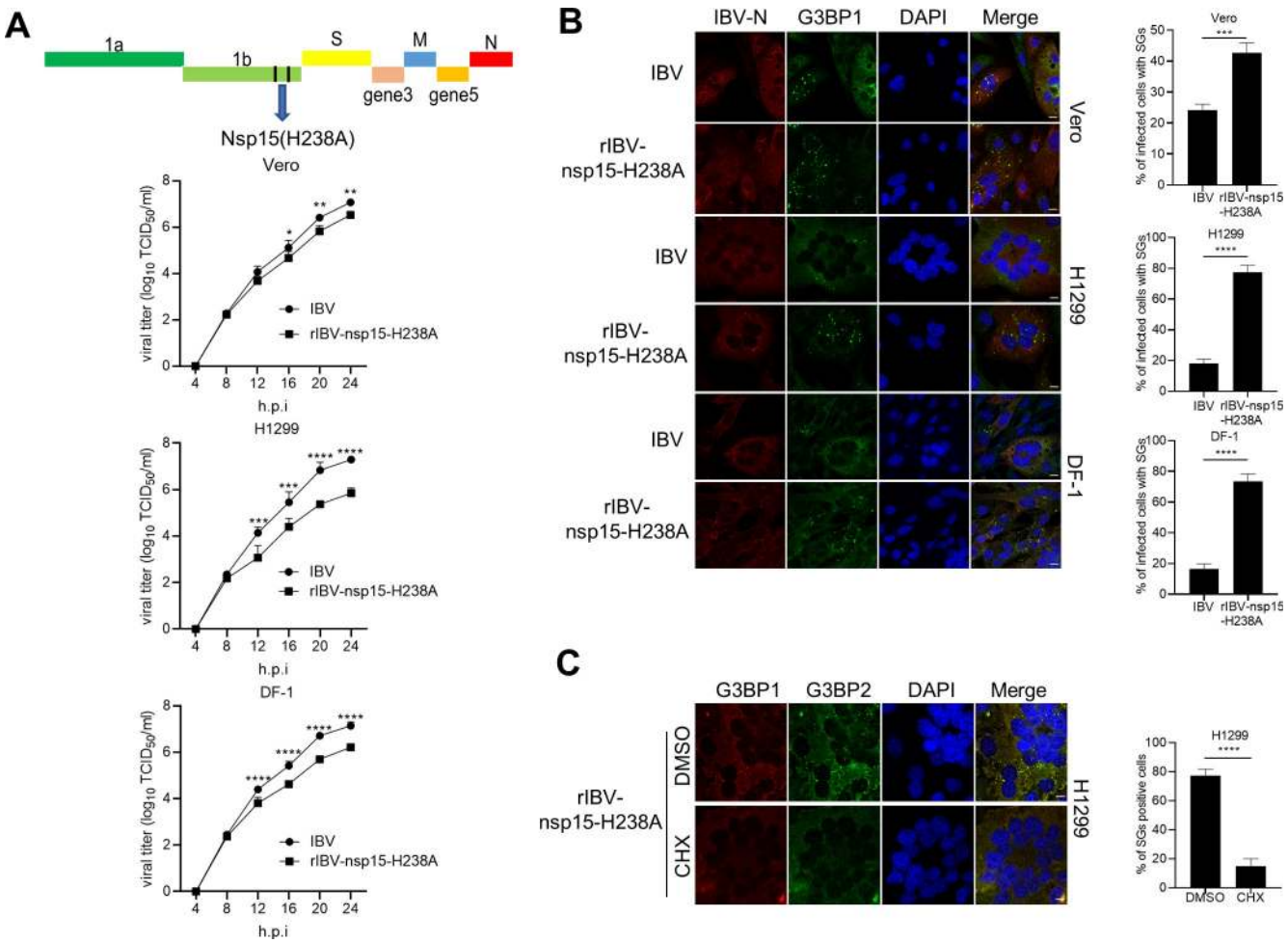

Fig 8. Nsp15-defective recombinant virus rIBV-nsp15-H238A greatly induces canonical SGs. (A) Schematic diagram of the nsp15 mutation site (H238-A) as described in the Material and methods, and the replication dynamics of IBV and rIBV-nsp15-H238A in Vero, H1299, and DF-1 cells. Cells were infected with IBV or rIBV-nsp15-H238A at an MOI of 1. Cell culture supernatants were collected at the indicated times at 4 h intervals and viral titers were determined by $TCID_{50}$ in Vero cells. The dot graphs showed the growth kinetics of IBV and rIBV-nsp15-H238A of three independent determinations, presented as the mean ± SD. (B) Vero, H1299, and DF-1 cells were infected with IBV or rIBV-nsp15-H238A at a MOI of 1 for 20 h, followed by immunostaining. Infected cells were identified with anti-IBN-N (red) and the SGs were detected with anti-G3BP1 (green). Cell nuclei were stained with DAPI (blue). The bar graphs on the right panel showed the percentage of SGs positive cells to total infected cells, which were calculated over 20 random fields, presented as the mean ± SD. *P* values were calculated by Student's test. ***, $P < 0.001$; ****, $P < 0.0001$. (C) H1299 cells were infected with rIBV-nsp15-H238A for 20 h and treated with 100 μg/ml of cycloheximide (CHX) or an equivalent volume of DMSO for 1 h, followed by immunostaining with anti-G3BP1 or anti-G3BP2 antibodies. The bar graphs showed the percentage of SGs positive cells to total cells, which were calculated over 20 random fields, presented as the mean ± SD. ****, $P < 0.0001$. The representative images of three independent experiments were shown. Scale bars: 10 μm.

https://doi.org/10.1371/journal.ppat.1008690.g008

absence of SGs during sodium arsenite stimulation and rIBV-nsp15-H238A infection (Fig 10A). Consistent with the high production of IFN-β (Fig 9B), rIBV-nsp15-H238A infection greatly stimulated the phosphorylation of TBK1 and IRF3 in G3BP1/2 positive cells (Fig 10B). As expected, in G3BP1/2 knock out cells, the levels of phospho-TBK1 and phospho-IRF3, triggered by rIBV-nsp15-H238A infection, were greatly decreased (Fig 10B); consequently, the transcription of *IFN-β* and ISG *IFIT-1* induced by rIBV-nsp15-H238A infection were significantly decreased (Fig 10C). Infection with rIBV-nsp15-H238A did not obviously activate p65, and in G3BP1/2$^{-/-}$ cells, phosphorylation level of p65 was slightly lower than in G3BP1 positive cells (Fig 10B). These results suggest that in response to rIBV-nsp15-H238A infection, the formation of SGs is mainly involved in eliciting IRF3-IFN signaling, not p65 signaling. It was

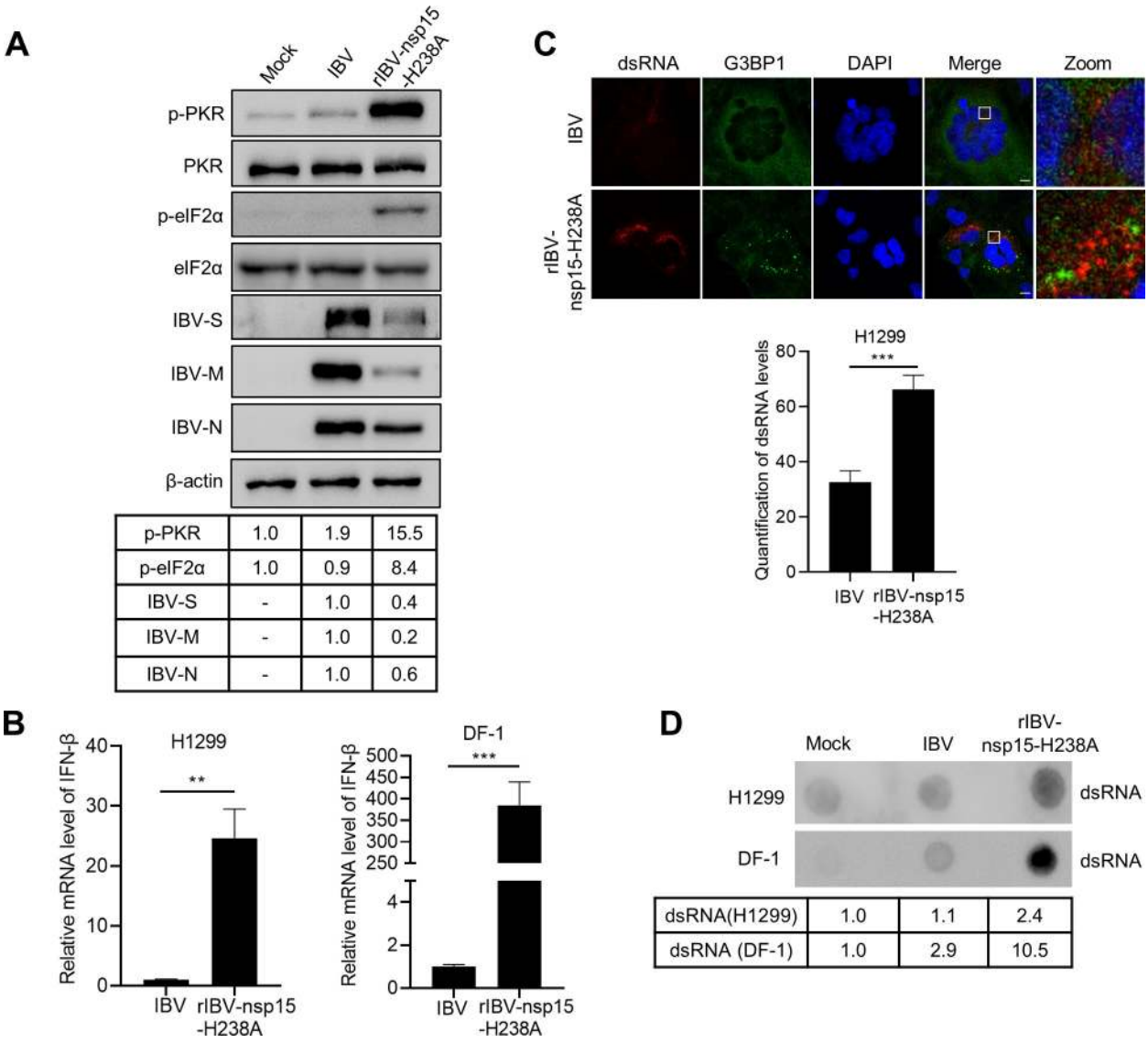

Fig 9. Nsp15-defective recombinant virus rIBV-nsp15-H238A strongly activates PKR by promoting dsRNA accumulation and eventually stimulates IFN response. (A) H1299 cells were mock-infected or infected with IBV or rIBV-nsp15-H238A of 1 MOI for 20 h. Cells were lysed for western blotting analysis to detect the level of p-PKR, PKR, p-eIF2α, eIF2α, IBV-S, IBV-M, IBV-N, and β-actin. Figures are representative of two independent experiments. The signals of protein bands were determined by Image J. The intensities of p-PKR or p-eIF2α were normalized to total PKR or eIF2α. The intensities of IBV-S, IBV-M, IBV-N were normalized to β-actin. The ratio of p-PKR and p-eIF2α in IBV infected cells to mock infected cells were shown as p-PKR and p-eIF2α, the ratio of IBV-S, IBV-N, and IBV-N of rIBV-nsp15-H238A to IBV were shown as IBV-S, IBV-M, and IBV-N. (B) H1299 and DF-1 cells were infected with IBV or rIBV-nsp15-H238A for 20 h, respectively. Total RNA was extracted and subjected to quantitative RT-PCR to determine the transcription of *IFN-β*. The bar graphs showed the relative mRNA level of IFN-β of three independent experiments, presented as mean ± SD. *P* values were calculated by Student's test. **, $P < 0.01$; ***, $P < 0.001$. (C) H1299 cells were infected with IBV or rIBV-nsp15-H238A for 20 h, followed by immunostaining. DsRNA (red) was detected with J2 antibody and G3BP1 or IBV-N (green) were determined with corresponding antibodies. The representative images of three independent experiments were shown. Bar graph showed the quantification of dsRNA levels by using Image J. ***, $P < 0.001$. Scale bars: 10 μm. (D) H1299 and DF-1 cells were infected with IBV or rIBV-nsp15-H238A for 20 h, respectively. Total RNA was extracted and 2 μg RNA was spotted onto a Hybond-N+ membrane. After UV-crosslink, the membrane was subjected to dsRNA-specific antibody J2 incubation. The representative blots of two independent experiments were shown. The signals of dots were determined by Image J. The ratio of dsRNA in IBV infected- or rIBV-nsp15-H238A-infected cells to mock-infected cells were shown.

https://doi.org/10.1371/journal.ppat.1008690.g009

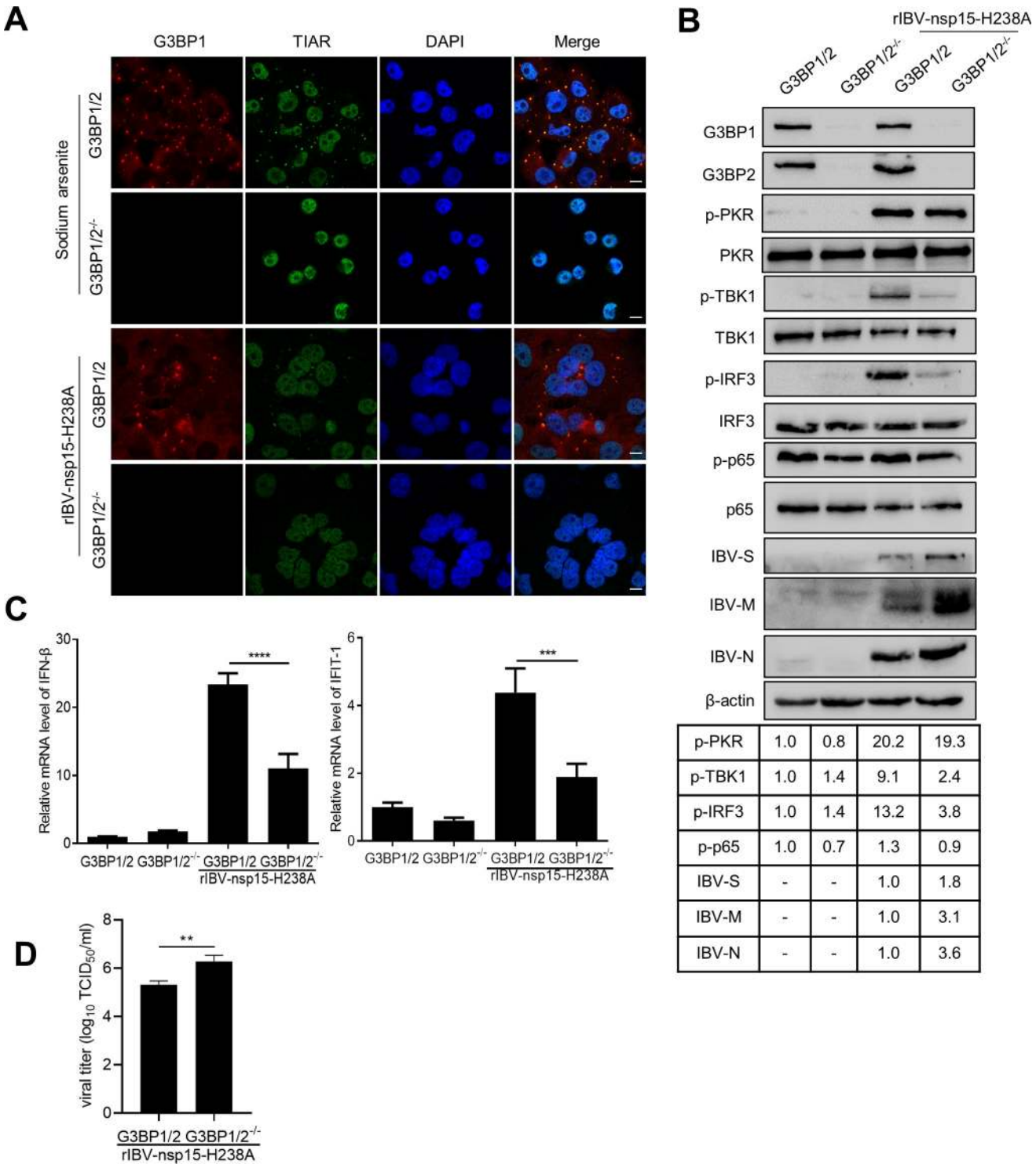

p-PKR	1.0	0.8	20.2	19.3
p-TBK1	1.0	1.4	9.1	2.4
p-IRF3	1.0	1.4	13.2	3.8
p-p65	1.0	0.7	1.3	0.9
IBV-S	-	-	1.0	1.8
IBV-M	-	-	1.0	3.1
IBV-N	-	-	1.0	3.6

Fig 10. Depletion of SGs scaffold proteins reduces rIBV-nsp15-H238A-triggered IRF3-IFN-β signaling. (A) H1299 G3BP 1/2 positive cells or H1299-G3BP1/2$^{-/-}$ cells were treated with sodium arsenite or infected with rIBV-nsp15-H238A for 20 h, followed by immunostaining with anti-G3BP1 (red) and anti-TIAR (green). The images are representative of three independent experiments. Scale bars: 10 μm. (B) H1299 G3BP1/2 positive cells and H1299-G3BP1/2$^{-/-}$ cells were mock-infected or infected with rIBV-nsp15-H238A for 20 h. Cell lysates were analyzed by western blot to detect G3BP1, G3BP2, p-PKR, PKR, p-TBK1, TBK1, p-IRF3, IRF3, p-p65, p65, IBV-S, IBV-M, IBV-N, and β-actin. The figures are representative of two independent experiments. The signals of protein bands were determined by Image J. The intensities of p-PKR, p-TBK1, p-IRF3, p-p65 were normalized to total PKR, TBK1, IRF3, p65, and the intensities of IBV-S, IBV-M, IBV-N were normalized to β-actin. The ratio of p-PKR, p-TBK1, p-IRF3, p-p65 in H1299-G3BP1/2$^{-/-}$ cells or rIBV-nsp15-H238A-infected cells to H1299 G3BP1/2 positive cells was were shown. The ratio of IBV-S, IBV-M, IBV-N in H1299-G3BP1/2$^{-/-}$

cells to those in H1299 G3BP1/2 positive cells were shown. (C) H1299 G3BP1/2 positive cells and H1299-G3BP1/2$^{-/-}$ cells were inoculated with rIBV-nsp15-H238A for 20 h and the induction of *IFN-β* and *IFIT-1* was quantified by quantitative RT-PCR. The levels of *IFN-β* or *IFIT-1* from three independent experiments were shown in the bar graphs, presented as mean ± SD. *P* values were calculated by Student's test. ***, $P < 0.001$; ****, $P < 0.0001$. (D) The supernatant from rIBV-nsp15-H238A-infected H1299 G3BP1/2 positive cells and H1299-G3BP1/2$^{-/-}$ cells was collected at 20 h.p.i. and virus titers were measured by $TCID_{50}$ assay. The bar graphs present the virus titers from three independent determinations, shown as mean ± SD. **, $P < 0.01$.

https://doi.org/10.1371/journal.ppat.1008690.g010

worth noting that G3BP1/2 knock out had no obvious effect on phospho-PKR levels (Fig 10B). Thus, SGs formation is not involved in PKR activation during IBV infection, although PKR activity has been reported to be enhanced and maintained by SG formation [64]. Interestingly, upon G3BP1/2 knock out, we observed higher levels of IBV-S, IBV-M, and IBV-N (Fig 10B) and in agreement, more progeny virus particles were produced, as evidenced by $TCID_{50}$ assay (Fig 10D). This is in line with our previous suggestion that activation of the type I IFN signaling might be the factor limiting rIBV-nsp15-H238A replication; failure to trigger an IFN-β response in G3BP1/2 knock out cells, however, promotes virus replication.

To investigate whether the involvement of SGs in IRF3-IFN signaling is restricted to specific virus infection, we examined the IRF3-IFN signaling upon poly I:C stimulation. Results showed that in G3BP1/2 positive cells, poly I:C strongly stimulated phosphorylation of IRF3 and to a lesser extent of TBK1 (Fig 11A), and promoted IRF3 nuclear translocation (Fig 11B, 34% of total cells display nuclear IRF3); however, in the absence of G3BP1/2, poly I:C stimulation led to reduced TBK1 phosphorylation, and to a greater extent, reduced IRF3 phosphorylation (Fig 11A) and nuclear translation (Fig 11B, 9% of total cells with nuclear IRF3). As a consequence, transcription of *IFN-β* and *IFIT-1* was significantly decreased upon poly I:C stimulation in G3BP1/2 knock out cells (Fig 11C). Again, it was noted that poly I:C greatly stimulated phosphorylation of PKR, knock out of G3BP1/2 had no effect on the level of phospho-PKR (Fig 11A). Altogether, these results demonstrate that SGs positively regulate IFN response and that such a mechanism is not restricted to a specific virus infection.

Aggregation of PRRs and signaling intermediates to SGs during IBV infection

A previous report showed that the dsRNA sensors PKR, MDA5, and RIG-I are located to SG and sense dsRNA [29]. In this study, we examined the subcellular localization of PRRs and signaling intermediates during IBV infection. In the small proportion of IBV-infected cells that displayed the presence of SGs, PKR, MDA5, TLR3 and MAVS aggregated and colocalized with G3BP1 granules (Fig 12A). These results demonstrate that SGs indeed recruit PRRs and their signaling intermediates during IBV infection. We further examined the subcellular location of signaling intermediates, results showed that TRAF3, TRAF6, TBK1, and IKKε all aggregated to G3BP1 granules (Fig 12B). These data, combined with the positive role on IRF3-IFN signaling, demonstrate that SGs may function as a platform for PRRs and downstream signaling intermediates.

Discussion

SGs formation or inhibition has been reported for different groups of coronaviruses: MHV and TGEV induce SGs or SG-like granules [39,40], whereas MERS-CoV does not [37,38], and IBV was reported to induce SGs formation but only in 20% of infected Vero cells [43] Yet, the biological significance of SGs in coronavirus replication is unclear. In this study, we report that IBV indeed induces SGs formation in a small proportion of infected cells and it does so not only in mammalian (Vero and H1299) cells, but also in chicken DF-1 cells. Furthermore,

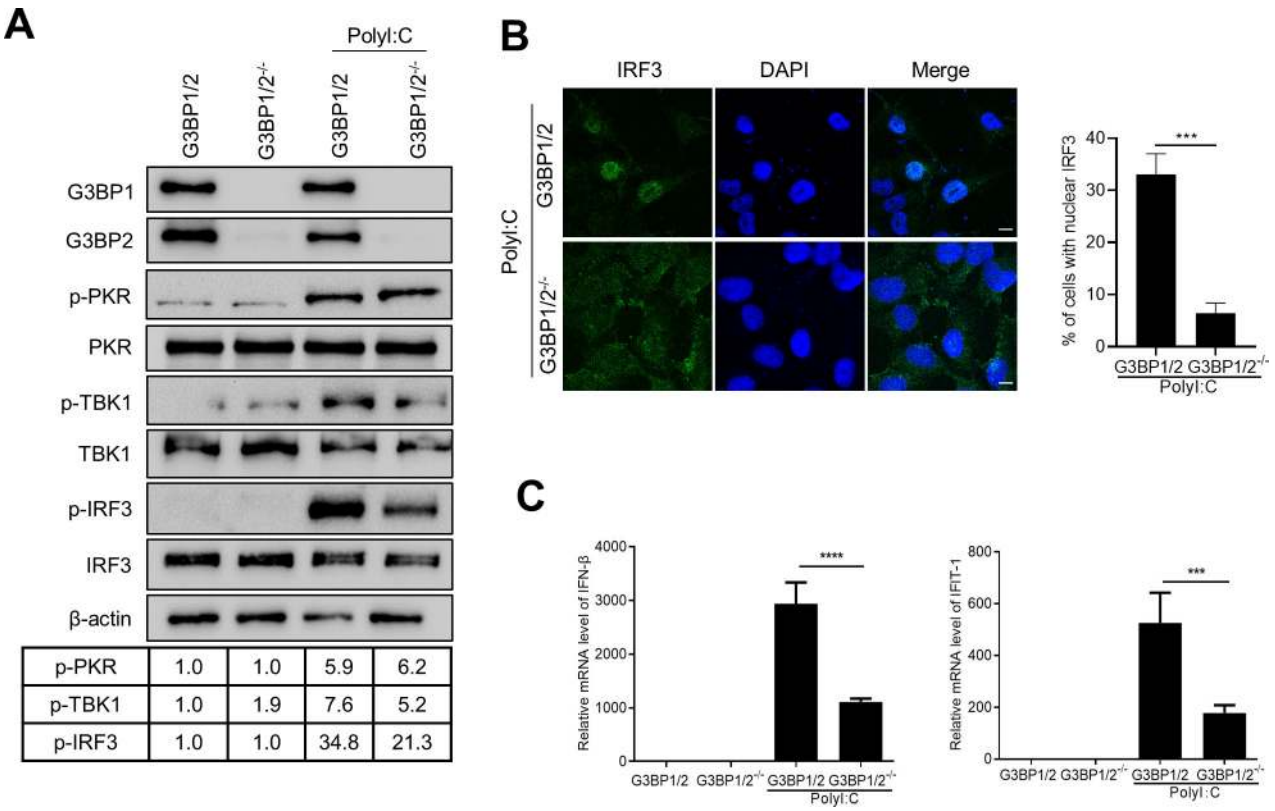

Fig 11. Depletion of SGs scaffold proteins reduces poly I:C-induced IRF3-IFN-β signaling. (A) H1299 G3BP1/2 positive cells and H1299-G3BP1/2$^{-/-}$ cells were transfected with poly I:C (1 μg/ml) for 6 h. The levels of p-PKR, PKR, G3BP1, G3BP2, p-TBK1, TBK1, p-IRF3, IRF3, and actin were determined by Western blot analysis. Images are representative of two independent experiments. The signals of protein bands were determined by Image J. The intensities of p-PKR, p-TBK1, p-IRF3 were normalized to total PKR, TBK1, IRF3. The ratio of p-PKR, p-TBK1, p-IRF3 in poly I:C transfected cells or H1299-G3BP1/2$^{-/-}$ cells to H1299 G3BP1/2 positive cells was were shown. (B) H1299 G3BP1/2 positive cells and H1299-G3BP1/2$^{-/-}$ cells were transfected with poly I:C. The nuclear translocation of IRF3 was examined by immunostaining. Scale bars: 10 μm. Images are representative of three independent experiments. The bar graphs on the right panel indicate the percentage of nuclear IRF3 positive cells to total cells, which were calculated by 20 random fields, presented as mean ± SD. ***, $P < 0.001$. (C) H1299 G3BP1/2 positive cells and H1299-G3BP1/2$^{-/-}$ cells were transfected with poly I:C. The induction of *IFN-β* and *IFIT-1* was quantified by quantitative RT-PCR. The bar graphs show relative expression levels of *IFN-β* or *IFIT-1* from three independent experiments, presented as mean ± SD. ***, $P < 0.001$; ****, $P < 0.0001$.

https://doi.org/10.1371/journal.ppat.1008690.g011

consistent with previous reports [43], also in our study we found that IBV inhibits both eIF2α-dependent (heat shock, sodium arsenite) and -independent (NaCl) SGs formation. We also assessed SGs formation by PEDV infection, only 10%-20% of PEDV-infected Vero cells were SGs positive (S6 Fig). It was noted that in the context of IBV or PEDV infection, SGs positive cells displayed lower IBV/PEDV protein expression than SGs negative cells (S7 Fig). The inhibition of virus replication in SG positive cells might be due to the protein translation shutoff, not due to stronger IFN response, as Vero cells are IFN deficient. This result suggest that protein translation shut off contributes to the formation of SGs in the small proportion of infected cells, consistent with the slightly activation of PKR by IBV infection (Fig 2). Combined with the inhibition of SGs formation by MERS-CoV [38], our results suggest that inhibition of SG formation by coronavirus might be a conserved phenomenon, not only restricted to a specific coronavirus genus. Screening of viral proteins involved in inhibition of SGs formation, revealed that nsp15 is a specific stress response antagonist of coronavirus: overexpression of nsp15s from IBV, PEDV, TGEV, SARS-CoV, and SARS-CoV-2, resulted in disruption of both eIF2α-dependent and -independent SGs formation, which could be attributed to its endoribonuclease activity; abrogating nsp15 endoribonuclease function *in vivo* led to impaired IBV

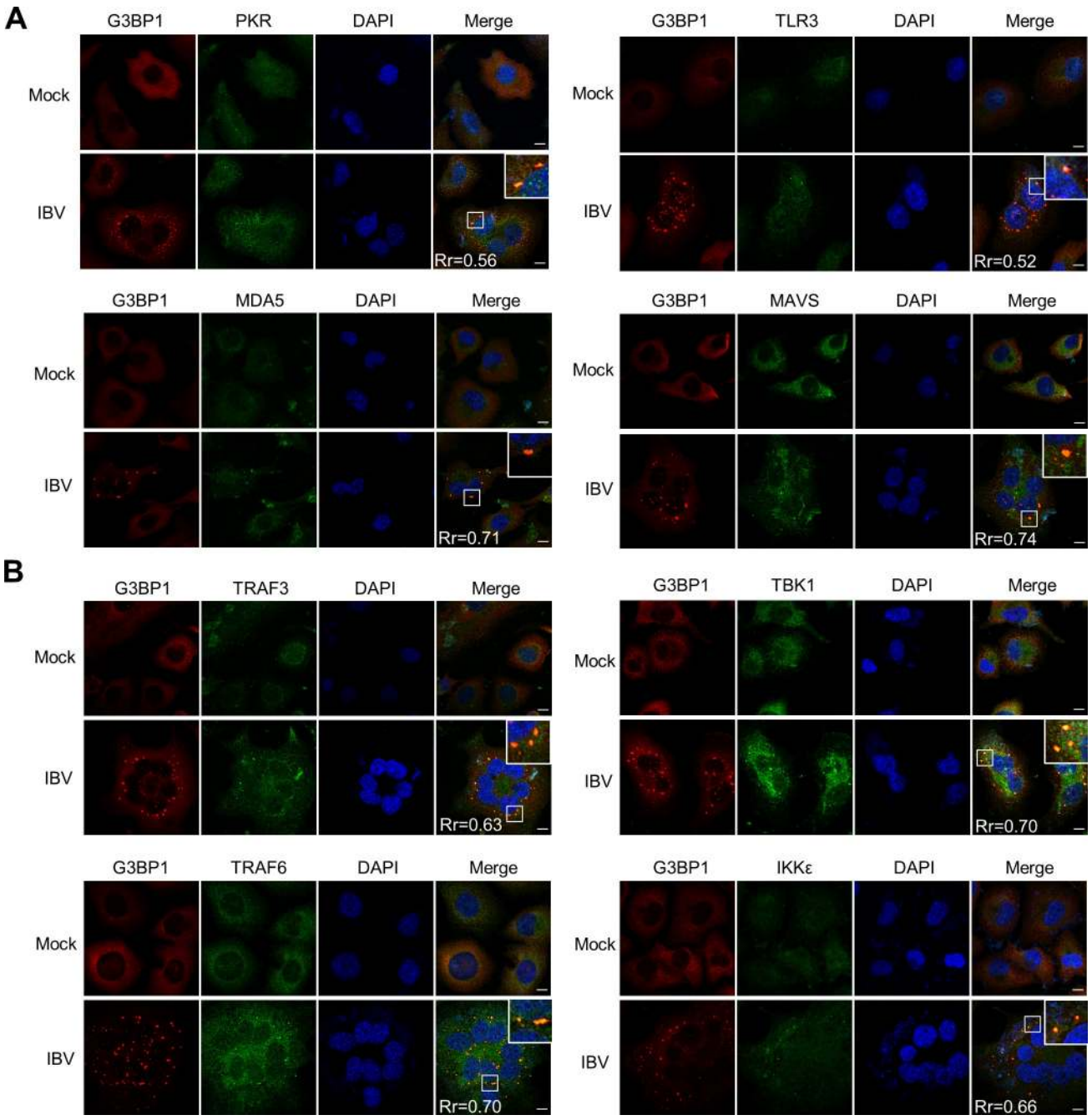

Fig 12. PRRs and innate immunity signaling intermediates aggregate to IBV-induced SGs. (A and B) H1299 cells were mock-infected or infected with IBV followed by immunostaining at 20 h.p.i.. Anti-G3BP1 (red) was used to monitor SGs formation, and PKR, MDA5, TLR3, MAVS, TRAF3, TRAF6, TBK1, IKKε (green) were detected with corresponding antibodies. Cell nuclei were stained with DAPI (blue). The Pearson's correlation coefficient was measured by using Image J. Scale bars, 10 μm. Images are representative of three independent experiments.

https://doi.org/10.1371/journal.ppat.1008690.g012

replication, efficient formation of SGs, accumulation of dsRNA, robust activation of PKR, and activation of IFN signaling. The absence of SGs in cells decrease the IFN response and partially restored the nsp15-defective IBV replication. Thus, we demonstrate that functional nsp15 is specifically required for efficient virus replication, by playing a role in preventing SG formation and the subsequent activation of IFN response.

Coronavirus nsp15 is a well characterized EndoU ribonuclease and has been demonstrated to be the main IFN antagonist for coronavirus to evade the host innate response [50,65]. It has uridylate-specific endoribonuclease activity on single-stranded RNA and dsRNA [66,67] and is considered an integral component of the RTC and co-localizes with viral RNA [68]. It was reported that mutations in the nsp15 active sites in MHV, SARS-CoV, and HCoV-229E lead to only a subtle defect in RNA synthesis and to a slight reduction in viral titers in fibroblast cell lines [69,70]. Recently, it was reported that MHV and HCoV-229E nsp15 is involved in evasion of dsRNA sensors MDA5, OAS, and PKR [51,52]. The nsp15-defective MHV exhibits severe replication defects in macrophages and is highly attenuated in mice [51,52]. In addition to MHV [51,52,65], the nsp15s from PEDV, SARS-CoV-2, SARS-CoV, and HCoV-229E are also characterized to be IFN antagonists [51,53,71–73]. By using a transcriptomics approaches to evaluate the host transcriptional response, Volk demonstrated that MHV nsp15 substantially contributes to the ability of coronaviruses to evade the host innate response in macrophages [65]. How does nsp15 evade the dsRNA sensors and antagonize IFN response? Coronavirus is a family of positive-stranded RNA viruses that replicate in the host cell cytoplasm. The viral RNA synthesis is performed in RTCs that include viral and cell proteins, connected with convoluted membranes and double membrane vesicles [74,75]. Replication of the coronavirus genome requires continuous RNA synthesis, whereas transcription is a discontinuous process unique among RNA viruses. Transcription includes a template switch during the synthesis of sub-genomic negative strand RNAs to add a copy of the leader sequence [76–78]. The negative strand RNA is the replication intermediate of genomic RNA and of sub-genomic RNA. During the replication and transcription process, positive and negative strand RNA form dsRNA. The amount of negative strand intermediates is approximately 10% of the positive strand RNA [79]. It is believed that the proper ratio of positive and negative stand RNA is important for efficient replication and transcription, as well as subsequent genome packaging and mRNA translation. As the negative strand RNA intermediates harbor a poly(U) sequence, which is complementary to the positive strand RNA poly (A) tail, we suppose that nsp15 targets to poly(U)-containing negative strand intermediates or dsRNA intermediates within stalled RTCs that are no longer active in viral RNA synthesis, thereby reducing the accumulation of dsRNA. This hypothesis is supported by our observation that, compared to wild type IBV, infection with nsp15-defective rIBV-nsp15-H238A leads to substantial accumulation of dsRNA intermediates (Fig 9C and 9D), with an increased ratio of negative strand:positive strand RNA (S5 Fig). During our manuscript preparation, this hypothesis is convincingly demonstrated by Hackbart et al., whose report shows that MHV and PEDV nsp15 cleaves the 5′-poly(U) from negative-sense viral RNA intermediates, and the poly(U) containing negative-sense viral RNA is sufficient to stimulate MDA5 [80]. In this way, nsp15 degrades the poly(U) negative strand RNA, contributes to evading the host innate immune response, thereby facilitating efficient replication of virus.

In addition to the well characterized anti-IFN function of nsp15, here, we describe a previously unrecognized role of nsp15 in the evasion of PKR activation and interference with SGs formation. RNA viruses that replicate via dsRNA intermediates can be detected as "non-self" by host dsRNA sensors: PKR, RIG-I, MDA5 and TLR3, eventually stimulating the production of type I IFN [24,25,27,81]. It is likely that dsRNA is shielded within double-membrane vesicles and replication intermediates are likely protected by the RTC and N protein. In this study, by generating nsp15-defective recombinant IBV, we found that compared to the wild type virus, infection with rIBV-nsp15-H238A lead to dsRNA accumulation, PKR activation, robust formation of SG as well as up-regulation of *IFN-β*, which ultimately coincided with impaired rIBV-nsp15-H238A replication. Therefore, IBV nsp15 acts as both stress and IFN responses antagonist, likely through removal of dsRNA intermediates, thereby efficiently evading

integrated stress and innate anti-viral host responses. The observation that IBV nsp15 acts as IFN antagonist is consistent with previous reports about MHV and HCoV-229E [51,52]. The evasion of PKR sensor by nsp15 was also reported by Kindler, which showed the increased phosphorylation of eIF2α and translational shutoff by nsp15-null MHV_{H277A} [51]. Thus, in MHV, nsp15 probably also plays a role in evading the formation of SGs, although it has been reported that MHV infection also triggers the formation of SGs [39]. Considering the conserved anti-SG function of nsp15s from IBV, PEDV, TGEV, SARS-CoV, and SARS-CoV-2, when they are expressed alone, nsp15 probably plays a main role in antagonize the integral stress response in coronaviruses. It has been well characterized here that in the context of virus infection, nsp15 evades the PKR-eIF2α-SG signaling by reducing dsRNA accumulation, however, when nsp15 expressed alone, how does nsp15 interfere with SGs formation?

Virus-encoded endoribonucleases not only modulate viral RNA, but also target the majority of cellular mRNAs, likely enabling viral mRNAs to better compete for limiting translation components and directing the cell from host to virus gene expression. Targeting host mRNA for degradation not only restricts host gene expression, but also subverts SGs by depleting the core component of SG, RNA. Thus, the ribonuclease is a unique strategy for viruses to subvert SGs. It has been well characterized that the herpes simplex virus 1 (HSV-1) and HSV2 employ the virion host shutoff (VHS) endoribonuclease to impede the SGs formation [82,83]. Infection with a mutant virus lacking VHS (ΔVHS) results in PKR activation and PKR-dependent SGs formation in multiple cell types [84,85]. Destabilization of host mRNAs by VHS may directly contribute to its disruption of SG formation [86]. In addition to cleaving the poly(U) negative strand RNA, coronavirus nsp15 probably also targets host mRNA and subsequently inhibits host protein translation. Interestingly, we previously showed that differently from beta-coronaviruses such as MHV and SARS-CoV [87,88], IBV shuts off host protein synthesis without affecting mRNA stability [89]. In the current study, when nsp15 was expressed alone, nsp15 enters into nucleus (Figs 4 and 5A–5C), which is different from the RTC localization in the context of virus infection. This prompt us to investigate the host factors that nsp15 targets to. We find that expression of nsp15s from different coronaviruses causes the nuclear localization of PABP1, which is attributed to its ribonuclease activity (Fig 7). Emerging evidence show that PABP1 accumulates in the nucleus when the cytoplasmic mRNA poly(A) to PABP1 ratio is decreased by prolonged transcriptional inhibition or transient ribonuclease expression, both of which reduce the cytoplasmic mRNA levels [60,90]; indirect inhibition of mRNA transcription, processing, or export also results in PABPs nuclear localization [60,91]. Although PABP1 is considered to be a *bona fide* SG component and SG marker, knock down or overexpression of PABP1 or PABP4 does not affect SG formation of mRNA localization to SGs [60]. Thus, PABP1 may passively localize to SGs as a consequence of mRNA accumulation at these foci. As PABP1 is not critical for SG formation, the nuclear localization of PABP1 probably is not the direct mechanism of inhibiting SGs formation by nsp15, probably is a byproduct phenomenon of other host factors targeted by nps15. In consideration of nsp15 ribonuclease activity is required, we speculate that nsp15 might target to host RNA to interfere with the chemically triggered SGs formation.

Several reports show that SGs serve as platform for viral dsRNA sensing by RLRs and subsequent activation of viral immune responses [92,93]. Recent studies report that several other IFN regulatory molecules, such as MEX3C, Riplet, DHX36 and Pumilios, also localize to SGs [94]. It is thus reasonable that viruses have evolved mechanisms to suppress SGs formation in order to promote their propagation. Influenza A virus (IAV) non-structural protein 1 (NS1) is reported to be involved in subversion of PKR-dependent SG formation [30]; importantly, during NS1-defective IAV infection, viral RNAs and nucleocapsid protein co-localize in SGs together with RIG-I, PKR and SGs markers G3BP1/TIAR; knock down of the G3BP1 or PKR

genes abrogated NS1-null IAV-induced IFN production, concomitantly with defects in SGs formation. Here, we find that wild type IBV triggers the formation of SGs only in 20% infected cells, and that PRRs (PKR, MDA5, TLR3) and signaling intermediates (MAVS, TRAF3, TRAF6, TBK1, IKKε) aggregate to the IBV-induced SGs. Nsp15-defective rIBV-nsp15-H238A robustly activates PKR, efficiently induces SGs formation, and strongly induced the transcription of *IFN-β*; but in SG core proteins-defective cells, either by rIBV-nsp15-H238A infection or poly I:C stimulation, the induction of *IFN-β* signaling is severely decreased. These data thus further confirm that SGs play a positive regulatory role in the IFN response, which is not restricted to a specific virus infection. These observations strongly suggest that the formation of SGs is critical for virus-induced antiviral innate immunity and SGs may function as a scaffold for viral RNA recognition by RLRs.

Altogether, there are several possibilities that may account for the lack of SGs formation upon transfection of nsp15 from different coronaviruses or infection with virus (Fig 13): (1) in the context of virus infection, nsp15 cleaves viral poly(U) negative strand RNA, reduces the accumulation of dsRNA, evades activating host sensor PKR and the formation of SGs; (2) nsp15 prevents the assembly of SGs or involved in the disassembly of SGs, by targeting host factors which are crucial for SGs assembly, probably by promoting the destruction of mRNAs present in polysome or free mRNA, by blocking the processing of pre-mRNA and nuclear export of mRNA, or by removal of mRNA from SGs. In consideration of nsp15 endoribonuclease is conserved within the families *Coronaviridae*, we speculate that, at least alpha-, beta-, and gamma-coronaviruses, employ similar mechanisms to antagonize the host anti-viral SGs formation. Altogether, this study firstly reports that coronavirus antagonizes the integral stress response through the endoribonuclease nsp15 and this is required for efficient virus replication. Future studies are needed to fully elucidate the mechanisms used by nsp15 to target to host factors and ultimately prevent the formation of SGs.

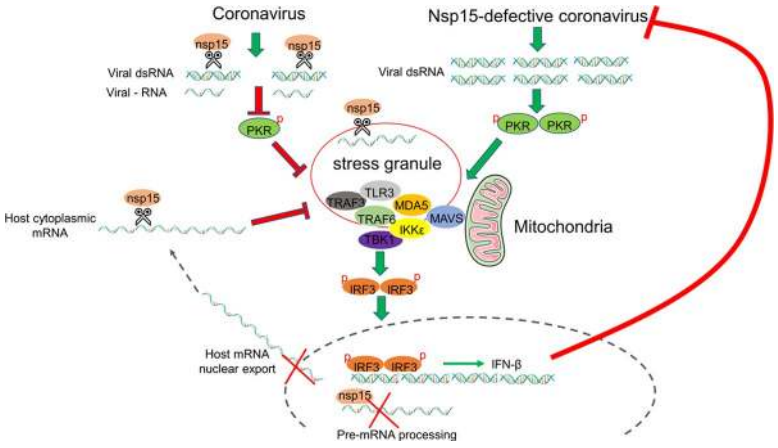

Fig 13. The working model of inhibition of anti-viral SG formation by coronavirus nsp15. Coronavirus genome replication and mRNA transcription produce negative strand RNA and dsRNA which contain poly(U) sequence. Nsp15 functions to cleave poly(U) negative strand RNA or dsRNA, reducing their accumulation. This prevents the activation of PKR and the formation of SGs. In parallel, nsp15 also targets to host factors, probably by cleaving host mRNA, or by interfering with host mRNA processing/nuclear export. This, in turns, prevents SGs assembly or promotes their disassembly. Defective nsp15 endoribonuclease activity in coronavirus, results in the accumulation of viral dsRNA, activation of PKR, and subsequent formation of SGs. The aggregation of PRRs and signaling intermediates to SGs facilitates the signaling transduction and IRF3 activation, finally inducing the expression of *IFN-β*. Production of *IFN*-β in turn, effectively limits coronavirus replication.

https://doi.org/10.1371/journal.ppat.1008690.g013

Materials and methods

Cells and viruses

Human non-small cell lung carcinoma cells H1299 were purchased from Cell Bank of Chinese Academy of Sciences and were maintained in Roswell Park Memorial Institute (RPMI) 1640 medium supplemented with 10% (v/v) fetal calf serum (FCS). Human cervical cancer cells HeLa, African green monkey kidney epithelial cells Vero, and chicken embryo fibroblasts DF-1 were purchased from ATCC and were grown in Dulbeco's modified eagle medium (DMEM) with 10% FCS. Porcine kidney epithelial cells LLC-PK1 and Swine testicular cells ST were kindly provided from Prof. Tongling Shan (Shanghai Veterinary Research Institute, CAAS), and were grown in minimum eagle's medium (MEM) and DMEM with 10% FCS respectively. IBV Beaudette strain was a gift from Prof. Dingxiang Liu's lab (South China Agricultural University). The recombinant virus rIBV-nsp15-H238A was constructed in our laboratory with the technical support of Prof. Shouguo Fang (Yangtze University, China), as further detailed below.

Antibodies and chemicals

Rabbit anti-IBV-S, rabbit anti-IBV-M, rabbit anti-IBV-N were the gifts from Prof. Dingxiang Liu's lab (South China Agricultural University, China). Mouse monoclonal anti-IBV-M was the gifts from Prof. Jiyong Zhou and Dr. Min Liao's lab (Zhejiang University, China). Mouse monoclonal anti-PEDV-N was the gift from Prof. Yanjun Zhou (Shanghai Academy of Agricultural Sciences, CAAS). Below we provide the list of all primary antibodies used, all of them directed against mammalian proteins; their dilution and eventual cross-reactivity to chicken proteins of interest are summarized in S1 Table. Rabbit anti-G3BP1 (ab181150), rabbit anti-G3BP2 (ab86135), rabbit anti-phospho-PKR (ab32036), rabbit anti-PABP1 (ab21060), rabbit anti-phospho-IRF3 (ab76493), and mouse anti-G3BP1 (ab56574) were purchased from Abcam; rabbit anti-TIAR (#8509), rabbit anti-PKR (#12297), rabbit anti-eIF2α (#5324), rabbit anti-phospho-eIF2α (#3398), rabbit anti-MDA5 (#5321), rabbit anti-TLR3 (#6961), rabbit anti-MAVS (#24930), rabbit anti-TARF3 (#61095), rabbit anti-TRAF6 (#8028), rabbit anti-IKKε (#3416), rabbit anti-TBK1 (#3504), rabbit anti-phospho-TBK1 (#5483), rabbit anti-IRF3 (#11904), rabbit anti-p65 (#8242), and rabbit anti-phospho-p65 (#3033) were purchased from Cell Signaling Technology; mouse anti-TIA-1 (sc-116247) was purchased from Santa Cruz; mouse anti-Flag (F1804) was purchased from Sigma; rabbit anti-β-actin (AC026), goat anti-rabbit IgG (H+L) (AS014), and goat anti-mouse IgG (H+L) (AS003) conjugated with HRP were from Abclonal; J2 mouse anti-dsRNA (10010200) was purchased from Scicons. Alexa Fluor goat anti-rabbit-488 (A-11034), Alexa Fluor goat anti-rabbit-594 (A-11037), Alexa Fluor goat anti-mouse-488 (A-11029), and Alexa Fluor goat anti-mouse-594 (A-11005) were obtained from Invitrogen. Sodium arsenite (S7400) and cycloheximide (239763-M) were purchased from Merck. Puromycin (ant-pr-1) and poly I:C (31852-29-6) were from InvivoGen.

Plasmids construction and transfection

The plasmids encoding IBV nsp2, nsp4, nsp5, nsp6, nsp7, nsp8, nsp9, nsp12, nsp15, nsp16, 3b, E, 5a, 5b, M, N and PEDV nsp15 were generated by amplification of cDNA from IBV Beaudette-infected or PEDV HLJBY-infected Vero cells using corresponding primers (S2 Table) and cloned into PXJ40F. The restriction endonuclease sites for most inserts are *BamH* I and *Xho* I, while the restriction endonuclease sites for M are *EcoR* I and *Xho* I. TGEV nsp15 was amplified by specific primers targeted cDNA which was a gift from Prof. Bin Li, Jiangsu Academy of Agricultural Sciences and then cloned into PXJ40F. PXJ40F encoding SARS-CoV-nsp15 or

SARS-CoV-2-nsp15 were synthesized and purchased from Sangon Biotech. The catalytic mutant plasmids of nsp15 were cloned by using Mut Express II Fast Mutagenesis Kit V2 (Vazyme). The mutagenesis primers are shown in S2 Table.

Cells were seeded on glass coverslips in a 24 wells cluster (25,000 cells/well). The indicated plasmids were transfected into cells using Fugene HD (Promega) according to the manufacturer's handbook. Briefly, 0.5 μg plasmid and 1.5 μl Fugene HD (m/v = 1:3) were diluted and incubated in 0.25 ml Opti-MEM (Gibco). After 5 min, plasmid and Fugene HD were mixed and incubated at room temperature for 15 min, allowing the formation of lipid-plasmid complex. Finally, the complex was added to the cultured cells and incubated for 24 h.

Indirect immunofluorescence and confocal microscopy

Cells were seeded on glass coverslips in a 24 wells cluster (25,000 cells/well) and the next day were transfected with various plasmids, infected with virus, or transfected with poly I:C (0.25 μg/well). At the indicated time points, cells were treated with heat shock (50˚C, 20 min), sodium arsenite (1 mM, 30 min), NaCl (200 mM, 50 min), or cycloheximide (100 μg/ml, 1 h), in the latter case DMSO was used as negative control. Cells were then fixed with 4% paraformaldehyde in PBS for 15 min at room temperature. After three washes with PBS, cells were permeabilized with 0.5% Triton X-100 in PBS for 15 min and incubated in blocking buffer (3% BSA in PBS) for 1 h. Cells were incubated with the primary antibody diluted in blocking buffer (as indicated in S1 Table) overnight at 4˚C, followed by incubation with Alexa Fluor conjugated secondary antibody diluted with 1:500 in blocking buffer for 1 h at 37˚C. In case of double staining, cells were incubated with a different unconjugated primary antibody, followed by incubation with the corresponding conjugated secondary antibody and incubated as described before. Between and after each incubation step, the cell monolayer was washed three times with blocking buffer. DAPI was then applied to stain nuclei for 15 min. Finally, cells were washed once with PBS and examined by Zeiss LSM880 confocal microscope.

Quantitative RT-PCR analysis

Total cellular RNAs were extracted using Trizol reagent (Ambion). cDNAs were synthesized from 2μg total RNA using oligo(dT) primers and M-MLV reverse transcriptase system (Promega). cDNA was used as template for quantitative PCR using a Bio-Rad CFX-96 real time PCR apparatus and SYBR green master mix (Dongsheng Biotech). PCR conditions were as follow: an initial denaturation at 94˚C for 3 min, 40 cycles of 94˚C for 15 s, 60˚C for 15 s and 72˚C for 20 s. The specificity of the amplified PCR products was confirmed by melting curve analysis after each reaction. The primers used were: for human *IFN-β*, 5'-GCTTGGATTC CTACAAAGAAGCA-3' (F) and 5'-ATAGATGGTCAATGCGGCGTC-3' (R); for human *IFIT-1*, 5'-GCCATTTTCTT TGCTTCCCCT-3' (F) and 5'-TGCCCTTTTGTAGCCTCC TT G-3' (R); for human *β-actin*, 5'-GATCTGGCACCACACCTTCT-3' (F) and 5'-GGGGTGT TGAAGGTC TCAAA-3' (R); for chicken *β-actin*, 5'-CCAGACATCAGGGTGTGATGG-3' (F) and 5'-CTCCATATCATCCCAGTTGGTGA-3' (R); for chicken *IFN-β*, 5'- GCTCTCA CCACCACCTTCTC-3' (F) and 5'- GCTTGCTTCTTGTCCTTGCT-3' (R); for IBV positive strand RNA: 5'-GTCTATCGCCAGGGAAATGTCT-3' (F) and 5'-GTCCTAGTGCTGTAC CCTCG-3'(R), which target to 3' untranslated region of virus genome; for IBV negative strand RNA: 5'-GTCCTAGTGCTGTACCCTCG-3' (F) and 5'-GTCTATCGCCAGGGAAATGTC T-3'(R), which target to 5' sequence of virus negative strand RNA. The relative expression ofeach gene or virus RNA was normalized to *β-actin* mRNA levels and calculated using the $2^{-\Delta\Delta CT}$ method. All assays were performed in triplicate and the results are expressed as the mean ± standard deviations.

Western blotting analysis

Cells were lysed in 2x protein loading buffer (20 mM Tris-HCl, 2% SDS, 100 mM DTT, 20% glycerol, 0.016% bromophenol blue). Cell debris was pelleted at 15000xg for 10 min and 10 μg of the cleared cell lysates were resolved on a 10% SDS-PAGE and transferred to 0.45 μm nitrocellulose membrane (GE life Sciences). Membranes were blocked in blocking buffer (5% non-fat milk, TBS, 0.1% Tween 20) for 1 h, followed by incubation with primary antibody diluted in blocking buffer as indicated in S1 Table overnight at 4˚C. The membranes were then incubated with secondary antibodies diluted in blocking buffer as indicated in S1 Table for 1 h at room temperature. Between and after the incubations, membranes were washed three time with washing buffer (0.1% Tween in TBS). The signals were developed with luminol chemiluminescence reagent kit (Share-bio) and detected using Tanon 4600 Chemiluminescent Imaging System (Bio Tanon).

DsRNA dot blot

H1299 or DF-1 cells were mock-infected or infected with IBV or rIBV-nsp15-H238A at 1 MOI for 20 h. Total RNA was extracted by using Trizol according to the manufacturer's protocol. 2 μg RNA was spotted on Hybond-N+ membrane (GE Healthcare) and followed with UV crossed-linking (120 mJ/cm^2) by using SCIENTZ 03-II (Scientz Biotech). After blocking with 5% non-fat milk dissolved in DEPC treated TBS, the membrane was incubated with mouse anti-dsRNA J2 antibody overnight at 4˚C, followed by incubation with goat anti-mouse secondary antibody for 1 h. Between and after the incubations, membranes were washed three time with washing buffer (0.1% Tween in TBS). The dsRNA signals were developed with luminol chemiluminescence reagent kit (Share-bio) and detected using Tanon 4600 Chemiluminescent Imaging System (Bio Tanon).

Quantification of SGs formation and IRF3 nuclear translocation

For quantification of SGs formation, images from 20 random high-powered fields were captured. The number of infected cells (IBV-N positive) in the acquired fields was counted. Cells displaying IBV-N expression and G3BP1 foci were counted as positive for SGs formation. The relative percentage of infected cells showing SGs formation was calculated by: cells positive with G3BP1 granules and IBV-N divided by cells positive with IBV-N × 100%. Similarly, for quantification of nuclear IRF3, 20 random high-powered fields were captured, and the percentage of cells displaying nuclear IRF3 to total cells was calculated.

Generation of G3BP1/2 knock out cell

Lenti CRISPRv2 was ligated with a pair of guide sequences targeting G3BP1/2 exon 1 which were designed by Zhang'lab (https://zlab.bio/guide-design-resources). The sgRNA of G3BP1 is 5'- CACCGTGTCCGTAGACTGCATCTGC-3' and G3BP2 is 5'- CACCGTACTTTGCTGAA TAAAGCTC-3'. The recombinant plasmid (14.5 μg), together with the packaging plasmids psPAX2 (14.5 μg) and pMD2.G (10 μg), were transfected into 70% confluence of HEK 293T cells in a 10 cm dish with Fugene (m/v = 1:3) to package lentiviruses. The supernatants containing lentiviruses were collected at 48 h post-transfection and concentrated by centrifugation (2000 x rpm, 15 min). H1299 cells were then infected with lentiviruses containing 8 μg/ml polybrene. After 48 h.p.i., puromycin (2 μg/ml) was applied to select for G3BP knockout cells. The G3BP1 and G3BP2 stably knockout cells were obtained after 5–6 passages and the absence of G3BP1/2 expression was confirmed by Western blot analysis and genome sequencing.

Construction of recombinant virus rIBV-nsp15-H238A

Plasmids pKTO-IBV-A, pGEM-IBV-B, pXL-IBV-C, pGEM-IBV-D, pGEM-IBV-E bearing IBV Beaudette fragment A, B, C, D and E covering the full-length genome (NC_001451.1) (see S3 Table) and plasmid pKTO-IBV-N containing N gene and 3'-UTR are generous gifts from Prof. Shouguo Fang, Yangtze University. Nsp15-H238A mutation was introduced by using Mut Express II Fast Mutagenesis Kit V2 on pGEM-IBV-D (primers sequences were shown in S2 Table). The *Bsa* I/*BsmB* I digested products of pKTO-IBV-A and pGEM-IBV-B were ligated by T4 ligase overnight, and the *Bsa* I/*BsmB* I digested products of C, D and E were ligated overnight. The AB and CDE were then ligated overnight to get the full-length cDNA genome with nsp15-H238A(AB+CDE). The full-length cDNA and *EcoR* I digested pKTO-IBV-N were subjected to *in vitro* transcription using T7 transcription kit (Promega), respectively, and added with cap structure using m7G (5') ppp (5') G RNA cap (New England biolabs). Next, the capped full-length RNA and IBV-N transcripts dissolved in 400 μl PBS were co-transfected into Vero cells by electroporation (450 v, 50 μF, 3 ms, GenePulser Xcell, BIO-RAD). After 48 h, the supernatant was collected and used to inoculate new Vero cells. When syncytia appeared, the supernatant was collected again and passaged on Vero cells for 3 to 5 times. Finally, the virus-containing medium was collected and sequenced. Viral titer was determined by $TCID_{50}$.

One step growth curve and Tissue culture infectious dose 50 ($TCID_{50}$) assay

Virus yield in the supernatant of rIBV-nsp15-H238A infected G3BP1/2 positive H1299 cells and G3BP1/2$^{-/-}$ H1299 cells were determined by $TCID_{50}$ assay. Briefly, the supernatant was serially diluted in 10-fold using serum free medium and inoculated to 70% confluence of Vero cells in 96 well plates. The virus and cells were incubated at 37˚C for 4 days. The cytopathogenic effect was observed after 4 days infection and the $TCID_{50}$ was calculated by Reed and Munch mathematical analysis [95].

One step growth curve of IBV and rIBV-nsp15-H238A in Vero, H1299, and DF-1 cells were infected with IBV or rIBV-nsp15-H238A at an MOI of 1. The cell culture supernatants were collected at 4, 8, 12, 16, 20, 24 h.p.i., respectively. The viral titers were determined by $TCID_{50}$ in Vero cells.

Statistical analysis

The statistical analysis was analyzed with Graphpad Prism8 software. The data showed as mean ± standard deviation (SD) of three independent experiments. Significance was determined with Student's test. P values < 0.05 were treated as statistically significant.

Densitometry

Image J program (NIH, USA) was used to quantify the intensities of corresponding bands of western blots, dsRNA dot blot, the intensity of dsRNA signal in immunofluorescence images, and Pearson's correlation coefficient of signals in immunofluorescence images, according to the manufacturer's instruction.

Supporting information

S1 Fig. The SGs induced by IBV are sensitive to cycloheximide treatment. (A) H1299 and DF-1 cells were infected with IBV Beaudette strain for 20 h and treated with 100 μg/ml of cycloheximide (CHX) or with an equivalent volume of DMSO for 1 h, followed by

immunostaining with anti-G3BP1 and anti-IBV-N antibodies. Shown are representative images of two independent experiments. Scale bars: 10 μm. (B) Quantification of the percentage of SGs positive cells to total IBV-infected cells in the context of DMSO treatment or cycloheximide (CHX) treatment. The bar graphs showed the percentage of SG positive cells to total infected cells of three independent experiments, which was counted over 20 random fields, presented as the mean ± SD. *, $P< 0.1$.
(TIF)

S2 Fig. Alignment of the catalytic core domain of nsp15s from different coronaviruses and XendoU of X. laevis. Catalytical sites were shown (*). Abbreviations: IBV, infectious bronchitis virus; PDCoV, porcine delta coronavirus; MHV, mouse hepatitis virus; HCoV-HKU1, human coronavirus HKU1; HCoV-OC43, human coronavirus OC43; SARS-CoV, severe acute respiratory syndrome coronavirus; SARS-CoV-2, severe acute respiratory syndrome coronavirus-2; MERS-CoV, Middle East respiratory syndrome coronavirus; HCoV-229E, human coronavirus 229E; HCoV-NL63, human coronavirus NL63; PEDV, porcine epidemic diarrhea virus; TGEV, transmissible gastroenteritis virus; XendU, endoribonuclease of X. laevis.
(TIF)

S3 Fig. Sodium arsenite treatment or rIBV-nsp15-H238A infection triggers UBAP2L foci, co-localized with G3BP1/2. H1299 cells were treated with 1 mM sodium arsenite for 30 min or infected with rIBV-nsp15-H238A for 20 h, followed by immunostaining with anti-G3BP1 (red) and anti-UBAP2L (green). Cell nuclei were stained with DAPI (blue). Shown are representative images of three independent experiments. Scale bars: 10 μm.
(TIF)

S4 Fig. Nsp15-defective recombinant virus rIBV-nsp15-H238A slightly increases the phosphorylation of PKR and eIF2α in Vero cells. (A) Vero cells were mock- infected or infected with IBV or rIBV-nsp15-H238A of 1 MOI for 20 h. Cells were lysed for western blotting analysis to detect the level of p-PKR, PKR, p-eIF2α, eIF2α, IBV-N, and β-actin. Shown are representative images of two independent experiments. The bands intensities were determined by Image J. The signals of p-PKR or p-eIF-2α were normalized to total PKR or total eIF2α, and the ratio of p-PKR or p-eIF-2α in IBV infected- or rIBV-nsp15-H238A infected-cells to mock-infected cells were shown. The signals of IBV-N were normalized to β-actin, and the ratio of rIBV-nsp15-H238A-N to IBV-N was shown.
(TIF)

S5 Fig. Nsp15-defective virus rIBV-nsp15-H238A increases the ratio of virus negative strand RNA to positive strand RNA. H1299 cells were infected with wild type IBV or rIBV-nsp15-H238A, respectively. At 8 h.p.i. and 20 h.p.i., cells were harvested and subjected to quantitative RT-PCR, for measuring the virus negative strand RNA intermediates and positive RNA, by using the primers indicated in Materials and Methods. The ratio of negative strand RNA to positive strand RNA of three independent experiments was calculated and shown in the bar graphs, presented as the mean ± SD. *, $P < 0.1$.
(TIF)

S6 Fig. PEDV prevents SGs formation in the majority of infected cells and abrogates eIF2α-dependent and -independent formation of SGs. (A) Vero cells were infected with PEDV HLJBY strain at an MOI of 1 or mock-infected. At the indicated time points, cells were subjected to immunostaining. Infected cells (red) were identified using a mouse anti-PEDV-N protein, SGs (green) were detected with rabbit anti-G3BP1 and cell nuclei were stained with DAPI (blue). Bar graphs in the right panel showed of the percentage of SGs/PEDV-N positive

cells to PEDV-N positive cells, which were counted over 20 random fields, mean ±SD. (B) Vero cells were infected with PEDV at an MOI of 1. At 20 h.p.i., cells received heat shock treatment (50˚C for 20 min) or 200 mM NaCl treatment for 50 min, followed by immunostaining. Shown are representative images of three independent experiments. Scale bars: 10 μm.
(TIF)

S7 Fig. SG positive cells display low IBV and PEDV replication. Vero cells were infected with IBV or PEDV at an MOI of 1 for 20 h, followed by immunostaining. Infected cells were identified with anti-IBV-M (red) or anti-PEDV-N (red) and the SGs with anti-G3BP1 (green) antibody. Cell nuclei were stained with DAPI (blue). Shown are representative images out of three independent experiments. Scale bars: 10 μm.
(TIF)

S1 Table. The dilution of primary antibodies and the cross reaction to chicken proteins.
(DOCX)

S2 Table. Primers used to construct plasmids.
(DOCX)

S3 Table. Plasmids for rIBV nsp15-H238A construction.
(DOCX)

Acknowledgments

We would like to thank Prof. Dingxiang Liu (South China Agricultural University, China) for providing the IBV Beaudette strain and the rabbit anti-IBV-N polyclonal antibody, and for his excellent scientific advice. We also grateful to Prof. Bin Li (Jiangsu Academy of Agricultural Sciences, China) for providing TGEV nsp15 cDNA, Dr. Changchao Huan (Yangzhou University, China) for the gift of PEDV HLJBY strain, Prof. Tongling Shan (Shanghai Academy of Agricultural Sciences, CAAS) for providing LLC-PK1 and ST cells, Prof. Yanjun Zhou (Shanghai Academy of Agricultural Sciences, CAAS) for providing the monoclonal PEDV N antibody, Prof. Jiyong Zhou and Dr. Min Liao (Zhejiang University, China) for providing IBV M monoclonal antibody.

Author Contributions

Conceptualization: Bo Gao, Xiaoqian Gong, Yingjie Sun, Maria Forlenza, Ying Liao.

Formal analysis: Bo Gao, Ying Liao.

Funding acquisition: Chan Ding, Ying Liao.

Investigation: Bo Gao, Xiaoqian Gong, Wenlian Weng, Huan Wang, Hongyan Chu.

Project administration: Chan Ding, Ying Liao.

Resources: Chunchun Meng, Lei Tan, Cuiping Song, Xusheng Qiu, Weiwei Liu.

Supervision: Shouguo Fang, Yingjie Sun, Maria Forlenza, Chan Ding, Ying Liao.

Writing – original draft: Bo Gao, Ying Liao.

Writing – review & editing: Maria Forlenza, Ying Liao.

References

1. Sparrer KM, Gack MU. Intracellular detection of viral nucleic acids. Current Opinion in Microbiology. 2015; 26:1–9. https://doi.org/10.1016/j.mib.2015.03.001 PMID: 25795286

2. Garcia MA, Meurs EF, Esteban M. The dsRNA protein kinase PKR: virus and cell control. Biochimie. 2007 Jun-Jul; 89(6–7):799–811. https://doi.org/10.1016/j.biochi.2007.03.001 PMID: 17451862

3. Vattem KM, Staschke KA, Zhu S, Wek RC. Inhibitory sequences in the N-terminus of the double-stranded-RNA-dependent protein kinase, PKR, are important for regulating phosphorylation of eukaryotic initiation factor 2alpha (eIF2alpha). Eur J Biochem. 2001 Feb; 268(4):1143–53. https://doi.org/10.1046/j.1432-1327.2001.01979.x PMID: 11179981

4. Jackson RJ, Hellen CU, Pestova TV. The mechanism of eukaryotic translation initiation and principles of its regulation. Nat Rev Mol Cell Biol. 2010 Feb; 11(2):113–27. https://doi.org/10.1038/nrm2838 PMID: 20094052

5. Lu L, Han AP, Chen JJ. Translation initiation control by heme-regulated eukaryotic initiation factor 2alpha kinase in erythroid cells under cytoplasmic stresses. Mol Cell Biol. 2001 Dec; 21(23):7971–80. https://doi.org/10.1128/MCB.21.23.7971-7980.2001 PMID: 11689689

6. McEwen E, Kedersha N, Song B, Scheuner D, Gilks N, Han A, et al. Heme-regulated inhibitor kinase-mediated phosphorylation of eukaryotic translation initiation factor 2 inhibits translation, induces stress granule formation, and mediates survival upon arsenite exposure. J Biol Chem. 2005 Apr 29; 280 (17):16925–33. https://doi.org/10.1074/jbc.M412882200 PMID: 15684421

7. Harding HP, Zhang Y, Bertolotti A, Zeng H, Ron D. Perk is essential for translational regulation and cell survival during the unfolded protein response. Mol Cell. 2000 May; 5(5):897–904. https://doi.org/10.1016/s1097-2765(00)80330-5 PMID: 10882126

8. Wek SA, Zhu S, Wek RC. The histidyl-tRNA synthetase-related sequence in the eIF-2 alpha protein kinase GCN2 interacts with tRNA and is required for activation in response to starvation for different amino acids. Mol Cell Biol. 1995 Aug; 15(8):4497–506. https://doi.org/10.1128/mcb.15.8.4497 PMID: 7623840

9. Deng J, Harding HP, Raught B, Gingras AC, Berlanga JJ, Scheuner D, et al. Activation of GCN2 in UV-irradiated cells inhibits translation. Curr Biol. 2002 Aug 6; 12(15):1279–86. https://doi.org/10.1016/s0960-9822(02)01037-0 PMID: 12176355

10. McCormick C, Khaperskyy DA. Translation inhibition and stress granules in the antiviral immune response. Nat Rev Immunol. 2017 Oct; 17(10):647–60. https://doi.org/10.1038/nri.2017.63 PMID: 28669985

11. Aulas A, Lyons SM, Fay MM, Anderson P, Ivanov P. Nitric oxide triggers the assembly of "type II" stress granules linked to decreased cell viability. Cell Death Dis. 2018 Nov 13; 9(11):1129. https://doi.org/10.1038/s41419-018-1173-x PMID: 30425239

12. Berchtold D, Battich N, Pelkmans L. A Systems-Level Study Reveals Regulators of Membrane-less Organelles in Human Cells. Mol Cell. 2018 Dec 20; 72(6):1035–49 e5. https://doi.org/10.1016/j.molcel.2018.10.036 PMID: 30503769

13. Aulas A, Fay MM, Lyons SM, Achorn CA, Kedersha N, Anderson P, et al. Stress-specific differences in assembly and composition of stress granules and related foci. J Cell Sci. 2017 Mar 1; 130(5):927–37. https://doi.org/10.1242/jcs.199240 PMID: 28096475

14. Kedersha NL, Gupta M, Li W, Miller I, Anderson P. RNA-binding proteins TIA-1 and TIAR link the phosphorylation of eIF-2 alpha to the assembly of mammalian stress granules. J Cell Biol. 1999 Dec 27; 147 (7):1431–42 https://doi.org/10.1083/jcb.147.7.1431 PMID: 10613902

15. Kedersha N, Cho MR, Li W, Yacono PW, Chen S, Gilks N, et al. Dynamic shuttling of TIA-1 accompanies the recruitment of mRNA to mammalian stress granules. J Cell Biol. 2000 Dec 11; 151(6):1257–68. https://doi.org/10.1083/jcb.151.6.1257 PMID: 11121440

16. Matsuki H, Takahashi M, Higuchi M, Makokha GN, Oie M, Fujii M. Both G3BP1 and G3BP2 contribute to stress granule formation. Genes Cells. 2013 Feb; 18(2):135–46. https://doi.org/10.1111/gtc.12023 PMID: 23279204

17. Jain S, Wheeler JR, Walters RW, Agrawal A, Barsic A, Parker R. ATPase-Modulated Stress Granules Contain a Diverse Proteome and Substructure. Cell. 2016 Jan 28; 164(3):487–98. https://doi.org/10.1016/j.cell.2015.12.038 PMID: 26777405

18. Chalupnikova K, Lattmann S, Selak N, Iwamoto F, Fujiki Y, Nagamine Y. Recruitment of the RNA helicase RHAU to stress granules via a unique RNA-binding domain. J Biol Chem. 2008 Dec 12; 283 (50):35186–98. https://doi.org/10.1074/jbc.M804857200 PMID: 18854321

19. Van Treeck B, Parker R. Emerging Roles for Intermolecular RNA-RNA Interactions in RNP Assemblies. Cell. 2018 Aug 9; 174(4):791–802. https://doi.org/10.1016/j.cell.2018.07.023 PMID: 30096311

20. Mollet S, Cougot N, Wilczynska A, Dautry F, Kress M, Bertrand E, et al. Translationally repressed mRNA transiently cycles through stress granules during stress. Mol Biol Cell. 2008 Oct; 19(10):4469–79. https://doi.org/10.1091/mbc.e08-05-0499 PMID: 18632980

21. Yamasaki S, Anderson P. Reprogramming mRNA translation during stress. Curr Opin Cell Biol. 2008 Apr; 20(2):222–6. https://doi.org/10.1016/j.ceb.2008.01.013 PMID: 18356035

22. Streicher F, Jouvenet N. Stimulation of Innate Immunity by Host and Viral RNAs. Trends Immunol. 2019 Dec; 40(12):1134–48. https://doi.org/10.1016/j.it.2019.10.009 PMID: 31735513

23. Rasmussen SB, Reinert LS, Paludan SR. Innate recognition of intracellular pathogens: detection and activation of the first line of defense. APMIS. 2009 May; 117(5–6):323–37. https://doi.org/10.1111/j.1600-0463.2009.02456.x PMID: 19400860

24. Chattopadhyay S, Sen GC. dsRNA-activation of TLR3 and RLR signaling: gene induction-dependent and independent effects. J Interferon Cytokine Res. 2014 Jun; 34(6):427–36. https://doi.org/10.1089/jir.2014.0034 PMID: 24905199

25. Kell AM, Gale M Jr. RIG-I in RNA virus recognition. Virology. 2015 May;479– 480:110–21. https://doi.org/10.1016/j.virol.2015.02.017 PMID: 25749629

26. Loo YM, Gale M Jr. Immune signaling by RIG-I-like receptors. Immunity. 2011 May 27; 34(5):680–92. https://doi.org/10.1016/j.immuni.2011.05.003 PMID: 21616437

27. Yoneyama M, Onomoto K, Jogi M, Akaboshi T, Fujita T. Viral RNA detection by RIG-I-like receptors. Curr Opin Immunol. 2015 Feb; 32:48–53. https://doi.org/10.1016/j.coi.2014.12.012 PMID: 25594890

28. Schneider WM, Chevillotte MD, Rice CM. Interferon-stimulated genes: a complex web of host defenses. Annu Rev Immunol. 2014 32:513–45. https://doi.org/10.1146/annurev-immunol-032713-120231 PMID: 24555472

29. Onomoto K, Jogi M, Yoo JS, Narita R, Morimoto S, Takemura A, et al. Critical role of an antiviral stress granule containing RIG-I and PKR in viral detection and innate immunity. PLoS One. 2012 7(8): e43031. https://doi.org/10.1371/journal.pone.0043031 PMID: 22912779

30. Khaperskyy DA, Hatchette TF, McCormick C. Influenza A virus inhibits cytoplasmic stress granule formation. FASEB J. 2012 Apr; 26(4):1629–39. https://doi.org/10.1096/fj.11-196915 PMID: 22202676

31. Simpson-Holley M, Kedersha N, Dower K, Rubins KH, Anderson P, Hensley LE, et al. Formation of antiviral cytoplasmic granules during orthopoxvirus infection. J Virol. 2011 Feb; 85(4):1581–93. https://doi.org/10.1128/JVI.02247-10 PMID: 21147913

32. Nelson EV, Schmidt KM, Deflube LR, Doganay S, Banadyga L, Olejnik J, et al. Ebola Virus Does Not Induce Stress Granule Formation during Infection and Sequesters Stress Granule Proteins within Viral Inclusions. J Virol. 2016 Aug 15; 90(16):7268–84. https://doi.org/10.1128/JVI.00459-16 PMID: 27252530

33. Visser LJ, Medina GN, Rabouw HH, de Groot RJ, Langereis MA, de Los Santos T, et al. Foot-and-Mouth Disease Virus Leader Protease Cleaves G3BP1 and G3BP2 and Inhibits Stress Granule Formation. J Virol. 2019 Jan 15; 93(2). https://doi.org/10.1128/JVI.00922-18 PMID: 30404792

34. Ye X, Pan T, Wang D, Fang L, Ma J, Zhu X, et al. Foot-and-Mouth Disease Virus Counteracts on Internal Ribosome Entry Site Suppression by G3BP1 and Inhibits G3BP1-Mediated Stress Granule Assembly via Post-Translational Mechanisms. Front Immunol. 2018 9:1142. https://doi.org/10.3389/fimmu.2018.01142 PMID: 29887867

35. Visser LJ, Langereis MA, Rabouw HH, Wahedi M, Muntjewerff EM, de Groot RJ, et al. Essential Role of Enterovirus 2A Protease in Counteracting Stress Granule Formation and the Induction of Type I Interferon. J Virol. 2019 May 15; 93(10). https://doi.org/10.1128/JVI.00222-19 PMID: 30867299

36. Yang X, Hu Z, Fan S, Zhang Q, Zhong Y, Guo D, et al. Picornavirus 2A protease regulates stress granule formation to facilitate viral translation. PLoS Pathog. 2018 Feb; 14(2):e1006901 https://doi.org/10.1371/journal.ppat.1006901 PMID: 29415027

37. Rabouw HH, Langereis MA, Knaap RC, Dalebout TJ, Canton J, Sola I, et al. Middle East Respiratory Coronavirus Accessory Protein 4a Inhibits PKR-Mediated Antiviral Stress Responses. PLoS Pathog. 2016 Oct; 12(10):e1005982. https://doi.org/10.1371/journal.ppat.1005982 PMID: 27783669

38. Nakagawa K, Narayanan K, Wada M, Makino S. Inhibition of Stress Granule Formation by Middle East Respiratory Syndrome Coronavirus 4a Accessory Protein Facilitates Viral Translation, Leading to Efficient Virus Replication. J Virol. 2018 Oct 15; 92(20). https://doi.org/10.1128/JVI.00902-18 PMID: 30068649

39. Raaben M, Groot Koerkamp MJ, Rottier PJ, de Haan CA. Mouse hepatitis coronavirus replication induces host translational shutoff and mRNA decay, with concomitant formation of stress granules and processing bodies. Cell Microbiol. 2007 Sep; 9(9):2218–29. https://doi.org/10.1111/j.1462-5822.2007.00951.x PMID: 17490409

40. Sola I, Galan C, Mateos-Gomez PA, Palacio L, Zuniga S, Cruz JL, et al. The polypyrimidine tract-binding protein affects coronavirus RNA accumulation levels and relocalizes viral RNAs to novel cytoplasmic domains different from replication-transcription sites. J Virol. 2011 May; 85(10):5136–49. https://doi.org/10.1128/JVI.00195-11 PMID: 21411518

41. Emmott E, Munday D, Bickerton E, Britton P, Rodgers MA, Whitehouse A, et al. The cellular interactome of the coronavirus infectious bronchitis virus nucleocapsid protein and functional implications for virus biology. J Virol. 2013 Sep; 87(17):9486–500. https://doi.org/10.1128/JVI.00321-13 PMID: 23637410

42. Cascarina SM, Ross ED. A proposed role for the SARS-CoV-2 nucleocapsid protein in the formation and regulation of biomolecular condensates. FASEB J. 2020 Jun 20. https://doi.org/10.1096/fj.202001351 PMID: 32562316.

43. Brownsword MJ, Doyle N, Brocard M, Locker N, Maier HJ. Infectious Bronchitis Virus Regulates Cellular Stress Granule Signaling. Viruses. 2020 May 14; 12(5). https://doi.org/10.3390/v12050536 PMID: 32422883

44. Narayanan K, Ramirez SI, Lokugamage KG, Makino S. Coronavirus nonstructural protein 1: Common and distinct functions in the regulation of host and viral gene expression. Virus Res. 2015 Apr 16; 202:89–100. https://doi.org/10.1016/j.virusres.2014.11.019 PMID: 25432065

45. Mielech AM, Kilianski A, Baez-Santos YM, Mesecar AD, Baker SC. MERS-CoV papain-like protease has delSGylating and deubiquitinating activities. Virology. 2014 Feb;450– 451:64–70. https://doi.org/10.1016/j.virol.2013.11.040 PMID: 24503068

46. Li SW, Wang CY, Jou YJ, Huang SH, Hsiao LH, Wan L, et al. SARS Coronavirus Papain-Like Protease Inhibits the TLR7 Signaling Pathway through Removing Lys63-Linked Polyubiquitination of TRAF3 and TRAF6. Int J Mol Sci. 2016 May 5; 17(5). https://doi.org/10.3390/ijms17050678 PMID: 27164085

47. Chen S, Tian J, Li Z, Kang H, Zhang J, Huang J, et al. Feline Infectious Peritonitis Virus Nsp5 Inhibits Type I Interferon Production by Cleaving NEMO at Multiple Sites. Viruses. 2019 12/30; 12:43. https://doi.org/10.3390/v12010043 PMID: 31905881

48. Zhu X, Fang L, Wang D, Yang Y, Chen J, Ye X, et al. Porcine deltacoronavirus nsp5 inhibits interferon-beta production through the cleavage of NEMO. Virology. 2017 Feb; 502:33–38. https://doi.org/10.1016/j.virol.2016.12.005 PMID: 27984784

49. Shi P, Su Y, Li R, Liang Z, Dong S, Huang J. PEDV nsp16 negatively regulates innate immunity to promote viral proliferation. Virus Res. 2019 May; 265:57–66. https://doi.org/10.1016/j.virusres.2019.03.005 PMID: 30849413

50. Deng X, Baker SC. An "Old" protein with a new story: Coronavirus endoribonuclease is important for evading host antiviral defenses. Virology. 2018 Jan 4. https://doi.org/10.1016/j.virol.2017.12.024 PMID: 29307596

51. Kindler E, Gil-Cruz C, Spanier J, Li Y, Wilhelm J, Rabouw HH, et al. Early endonuclease-mediated evasion of RNA sensing ensures efficient coronavirus replication. PLoS Pathog. 2017 Feb; 13(2): e1006195. https://doi.org/10.1371/journal.ppat.1006195 PMID: 28158275

52. Deng X, Hackbart M, Mettelman RC, O'Brien A, Mielech AM, Yi G, et al. Coronavirus nonstructural protein 15 mediates evasion of dsRNA sensors and limits apoptosis in macrophages. Proc Natl Acad Sci U S A. 2017 May 23; 114(21):E4251–E60. https://doi.org/10.1073/pnas.1618310114 PMID: 28484023

53. Deng X, van Geelen A, Buckley AC, O'Brien A, Pillatzki A, Lager KM, et al. Coronavirus Endoribonuclease Activity in Porcine Epidemic Diarrhea Virus Suppresses Type I and Type III Interferon Responses. J Virol. 2019 Apr 15; 93(8). https://doi.org/10.1128/JVI.02000-18 PMID: 30728254

54. Cavanagh D. Coronavirus avian infectious bronchitis virus. Vet Res. 2007 Mar-Apr; 38(2):281–97. https://doi.org/10.1051/vetres:2006055 PMID: 17296157

55. Zhang Q, Sharma NR, Zheng ZM, Chen M. Viral Regulation of RNA Granules in Infected Cells. Virol Sin. 2019 Apr; 34(2):175–91. https://doi.org/10.1007/s12250-019-00122-3 PMID: 31037644

56. Poblete-Duran N, Prades-Perez Y, Vera-Otarola J, Soto-Rifo R, Valiente-Echeverria F. Who Regulates Whom? An Overview of RNA Granules and Viral Infections. Viruses. 2016 Jun 28; 8(7). https://doi.org/10.3390/v8070180 PMID: 27367717

57. Dabo S, Maillard P, Collados Rodriguez M, Hansen MD, Mazouz S, Bigot DJ, et al. Inhibition of the inflammatory response to stress by targeting interaction between PKR and its cellular activator PACT. Sci Rep. 2017 Nov 23; 7(1):16129. https://doi.org/10.1038/s41598-017-16089-8 PMID: 29170442

58. Anderson P, Kedersha N. Stressful initiations. J Cell Sci. 2002 Aug 15; 115(Pt 16):3227–34 PMID: 12140254

59. Kedersha N, Panas MD, Achorn CA, Lyons S, Tisdale S, Hickman T, et al. G3BP-Caprin1-USP10 complexes mediate stress granule condensation and associate with 40S subunits. J Cell Biol. 2016 Mar 28; 212(7):845–60. https://doi.org/10.1083/jcb.201508028 PMID: 27022092

60. Burgess HM, Richardson WA, Anderson RC, Salaun C, Graham SV, Gray NK. Nuclear relocalisation of cytoplasmic poly(A)-binding proteins PABP1 and PABP4 in response to UV irradiation reveals mRNA-dependent export of metazoan PABPs. J Cell Sci. 2011 Oct 1; 124(Pt 19):3344–55. https://doi.org/10.1242/jcs.087692 PMID: 21940797

61. Desmyter J, Melnick JL, Rawls WE. Defectiveness of interferon production and of rubella virus interference in a line of African green monkey kidney cells (Vero). J Virol. 1968 Oct; 2(10):955–61. https://doi.org/10.1128/JVI.2.10.955-961.1968 PMID: 4302013

62. Cirillo L, Cieren A, Barbieri S, Khong A, Schwager F, Parker R, et al. UBAP2L Forms Distinct Cores that Act in Nucleating Stress Granules Upstream of G3BP1. Curr Biol. 2020 Feb 24; 30(4):698–707 e6. https://doi.org/10.1016/j.cub.2019.12.020 PMID: 31956030

63. Kint J, Fernandez-Gutierrez M, Maier HJ, Britton P, Langereis MA, Koumans J, et al. Activation of the chicken type I interferon response by infectious bronchitis coronavirus. J Virol. 2015 Jan 15; 89 (2):1156–67. https://doi.org/10.1128/JVI.02671-14 PMID: 25378498

64. Reineke LC, Lloyd RE. The stress granule protein G3BP1 recruits protein kinase R to promote multiple innate immune antiviral responses. J Virol. 2015 Mar; 89(5):2575–89. https://doi.org/10.1128/JVI.02791-14 PMID: 25520508

65. Volk A, Hackbart M, Deng X, Cruz-Pulido Y, O'Brien A, Baker SC. Coronavirus Endoribonuclease and Deubiquitinating Interferon Antagonists Differentially Modulate the Host Response during Replication in Macrophages. J Virol. 2020 May 18; 94(11). https://doi.org/10.1128/JVI.00178-20 PMID: 32188729

66. Bhardwaj K, Guarino L, Kao CC. The severe acute respiratory syndrome coronavirus Nsp15 protein is an endoribonuclease that prefers manganese as a cofactor. J Virol. 2004 Nov; 78(22):12218–24. https://doi.org/10.1128/JVI.78.22.12218-12224.2004 PMID: 15507608

67. Cao J, Wu CC, Lin TL. Turkey coronavirus non-structure protein NSP15—an endoribonuclease. Intervirology. 2008 51(5):342–51. https://doi.org/10.1159/000175837 PMID: 19023218

68. Snijder EJ, Decroly E, Ziebuhr J. The Nonstructural Proteins Directing Coronavirus RNA Synthesis and Processing. Adv Virus Res. 2016 96:59–126. https://doi.org/10.1016/bs.aivir.2016.08.008 PMID: 27712628

69. Kang H, Bhardwaj K, Li Y, Palaninathan S, Sacchettini J, Guarino L, et al. Biochemical and genetic analyses of murine hepatitis virus Nsp15 endoribonuclease. J Virol. 2007 Dec; 81(24):13587–97. https://doi.org/10.1128/JVI.00547-07 PMID: 17898055

70. Ulferts R, Ziebuhr J. Nidovirus ribonucleases: structures and functions in viral replication. RNA Biol. 2011 8(2):295–304. https://doi.org/10.4161/rna.8.2.15196 PMID: 21422822

71. Lei Y, Moore CB, Liesman RM, O'Connor BP, Bergstralh DT, Chen ZJ, et al. MAVS-mediated apoptosis and its inhibition by viral proteins. PLoS One. 2009 4(5):e5466. https://doi.org/10.1371/journal.pone.0005466 PMID: 19404494

72. Yuen CK, Lam JY, Wong WM, Mak LF, Wang X, Chu H, et al. SARS-CoV-2 nsp13, nsp14, nsp15 and orf6 function as potent interferon antagonists. Emerg Microbes Infect. 2020 Dec; 9(1):1418–28. https://doi.org/10.1080/22221751.2020.1780953 PMID: 32529952

73. Wu Y, Zhang H, Shi Z, Chen J, Li M, Shi H, et al. Porcine Epidemic Diarrhea Virus nsp15 Antagonizes Interferon Signaling by RNA Degradation of TBK1 and IRF3. Viruses. 2020 May 31; 12(6). https://doi.org/10.3390/v12060599 PMID: 32486349

74. Angelini MM, Akhlaghpour M, Neuman BW, Buchmeier MJ. Severe acute respiratory syndrome coronavirus nonstructural proteins 3, 4, and 6 induce double-membrane vesicles. MBio. 2013 Aug 13;4(4). https://doi.org/10.1128/mBio.00524-13 PMID: 23943763

75. Maier HJ, Hawes PC, Cottam EM, Mantell J, Verkade P, Monaghan P, et al. Infectious bronchitis virus generates spherules from zippered endoplasmic reticulum membranes. MBio. 2013 Oct 22; 4(5): e00801–13. https://doi.org/10.1128/mBio.00801-13 PMID: 24149513

76. Sola I, Almazan F, Zuniga S, Enjuanes L. Continuous and Discontinuous RNA Synthesis in Coronaviruses. Annu Rev Virol. 2015 Nov; 2(1):265–88. https://doi.org/10.1146/annurev-virology-100114-055218 PMID: 26958916

77. Madhugiri R, Fricke M, Marz M, Ziebuhr J. Coronavirus cis-Acting RNA Elements. Adv Virus Res. 2016 96:127–63. https://doi.org/10.1016/bs.aivir.2016.08.007 PMID: 27712622

78. Sola I, Mateos-Gomez PA, Almazan F, Zuniga S, Enjuanes L. RNA-RNA and RNA-protein interactions in coronavirus replication and transcription. RNA Biol. 2011 Mar-Apr; 8(2):237–48. https://doi.org/10.4161/rna.8.2.14991 PMID: 21378501

79. Sethna PB, Hofmann MA, Brian DA. Minus-strand copies of replicating coronavirus mRNAs contain antileaders. J Virol. 1991 Jan; 65(1):320–5. https://doi.org/10.1128/JVI.65.1.320-325.1991 PMID: 1985203

80. Hackbart M, Deng X, Baker SC. Coronavirus endoribonuclease targets viral polyuridine sequences to evade activating host sensors. Proc Natl Acad Sci U S A. 2020 Apr 7; 117(14):8094–103. https://doi.org/10.1073/pnas.1921485117 PMID: 32198201

81. Pindel A, Sadler A. The role of protein kinase R in the interferon response. J Interferon Cytokine Res. 2011 Jan; 31(1):59–70. https://doi.org/10.1089/jir.2010.0099 PMID: 21166592

82. Burgess HM, Mohr I. Defining the Role of Stress Granules in Innate Immune Suppression by the Herpes Simplex Virus 1 Endoribonuclease VHS. J Virol. 2018 Aug 1; 92(15). https://doi.org/10.1128/JVI.00829-18 PMID: 29793959

83. Finnen RL, Zhu M, Li J, Romo D, Banfield BW. Herpes Simplex Virus 2 Virion Host Shutoff Endoribonuclease Activity Is Required To Disrupt Stress Granule Formation. J Virol. 2016 Sep 1; 90(17):7943–55. https://doi.org/10.1128/JVI.00947-16 PMID: 27334584

84. Dauber B, Poon D, Dos Santos T, Duguay BA, Mehta N, Saffran HA, et al. The Herpes Simplex Virus Virion Host Shutoff Protein Enhances Translation of Viral True Late mRNAs Independently of Suppressing Protein Kinase R and Stress Granule Formation. J Virol. 2016 Jul 1; 90(13):6049–57. https://doi.org/10.1128/JVI.03180-15 PMID: 27099317

85. Sciortino MT, Parisi T, Siracusano G, Mastino A, Taddeo B, Roizman B. The virion host shutoff RNase plays a key role in blocking the activation of protein kinase R in cells infected with herpes simplex virus 1. J Virol. 2013 Mar; 87(6):3271–6. https://doi.org/10.1128/JVI.03049-12 PMID: 23302873

86. Elliott G, Pheasant K, Ebert-Keel K, Stylianou J, Franklyn A, Jones J. Multiple Posttranscriptional Strategies To Regulate the Herpes Simplex Virus 1 vhs Endoribonuclease. J Virol. 2018 Sep 1; 92(17). https://doi.org/10.1128/JVI.00818-18 PMID: 29925667

87. Huang C, Lokugamage KG, Rozovics JM, Narayanan K, Semler BL, Makino S. SARS coronavirus nsp1 protein induces template-dependent endonucleolytic cleavage of mRNAs: viral mRNAs are resistant to nsp1-induced RNA cleavage. PLoS Pathog. 2011 Dec; 7(12):e1002433. https://doi.org/10.1371/journal.ppat.1002433 PMID: 22174690

88. Kamitani W, Huang C, Narayanan K, Lokugamage KG, Makino S. A two-pronged strategy to suppress host protein synthesis by SARS coronavirus Nsp1 protein. Nat Struct Mol Biol. 2009 Nov; 16(11):1134–40. https://doi.org/10.1038/nsmb.1680 PMID: 19838190

89. Kint J, Langereis MA, Maier HJ, Britton P, van Kuppeveld FJ, Koumans J, et al. Infectious Bronchitis Coronavirus Limits Interferon Production by Inducing a Host Shutoff That Requires Accessory Protein 5b. J Virol. 2016 Aug 15; 90(16):7519–28. https://doi.org/10.1128/JVI.00627-16 PMID: 27279618

90. Kumar GR, Shum L, Glaunsinger BA. Importin alpha-mediated nuclear import of cytoplasmic poly(A) binding protein occurs as a direct consequence of cytoplasmic mRNA depletion. Mol Cell Biol. 2011 Aug; 31(15):3113–25. https://doi.org/10.1128/MCB.05402-11 PMID: 21646427

91. Dobrikova E, Shveygert M, Walters R, Gromeier M. Herpes simplex virus proteins ICP27 and UL47 associate with polyadenylate-binding protein and control its subcellular distribution. J Virol. 2010 Jan; 84(1):270–9. https://doi.org/10.1128/JVI.01740-09 PMID: 19864386

92. Yoneyama M, Jogi M, Onomoto K. Regulation of antiviral innate immune signaling by stress-induced RNA granules. J Biochem. 2016 Mar; 159(3):279–86. https://doi.org/10.1093/jb/mvv122 PMID: 26748340

93. Oh SW, Onomoto K, Wakimoto M, Onoguchi K, Ishidate F, Fujiwara T, et al. Leader-Containing Uncapped Viral Transcript Activates RIG-I in Antiviral Stress Granules. PLoS Pathog. 2016 Feb; 12(2): e1005444. https://doi.org/10.1371/journal.ppat.1005444 PMID: 26862753

94. Onomoto K, Yoneyama M, Fung G, Kato H, Fujita T. Antiviral innate immunity and stress granule responses. Trends Immunol. 2014 Sep; 35(9):420–8. https://doi.org/10.1016/j.it.2014.07.006 PMID: 25153707

95. McHenry EW, Reedman EJ, Sheppard M. The physiological properties of ascorbic acid: An effect upon the weights of guinea-pigs. Biochem. J. 1938 32(8):1302–04 https://doi.org/10.1042/bj0321302 PMID: 16746755